Atmos. Chem. Phys., 20, 7335–7358, 2020
https://doi.org/10.5194/acp-20-7335-2020

Atmospheric Chemistry and Physics
Open Access
EGU

Evaluating the impact of blowing-snow sea salt aerosol on springtime BrO and O_3 in the Arctic

Jiayue Huang[1], Lyatt Jaeglé[1], Qianjie Chen[1,a], Becky Alexander[1], Tomás Sherwen[2,3], Mat J. Evans[2,3], Nicolas Theys[4], and Sungyeon Choi[5,6]

[1]Department of Atmospheric Sciences, University of Washington, Seattle, WA 98115, USA
[2]Wolfson Atmospheric Chemistry Laboratories, Department of Chemistry, University of York, York YO10 5DD, UK
[3]National Centre for Atmospheric Science, University of York, York, YO10 5DD, UK
[4]Royal Belgian Institute for Space Aeronomy (BIRA-IASB), Brussels, Belgium
[5]Science Systems and Applications, Inc., Lanham, MD 20706, USA
[6]NASA Goddard Space Flight Center, Greenbelt, MD 20771, USA
[a]now at: Department of Chemistry, University of Michigan, Ann Arbor, MI 48109, USA

Correspondence: Lyatt Jaeglé (jaegle@uw.edu)

Received: 27 November 2019 – Discussion started: 30 January 2020
Revised: 17 April 2020 – Accepted: 18 May 2020 – Published: 25 June 2020

Abstract. We use the GEOS-Chem chemical transport model to examine the influence of bromine release from blowing-snow sea salt aerosol (SSA) on springtime bromine activation and O_3 depletion events (ODEs) in the Arctic lower troposphere. We evaluate our simulation against observations of tropospheric BrO vertical column densities (VCD_{tropo}) from the GOME-2 (second Global Ozone Monitoring Experiment) and Ozone Monitoring Instrument (OMI) spaceborne instruments for 3 years (2007–2009), as well as against surface observations of O_3. We conduct a simulation with blowing-snow SSA emissions from first-year sea ice (FYI; with a surface snow salinity of 0.1 psu) and multi-year sea ice (MYI; with a surface snow salinity of 0.05 psu), assuming a factor of 5 bromide enrichment of surface snow relative to seawater. This simulation captures the magnitude of observed March–April GOME-2 and OMI VCD_{tropo} to within 17 %, as well as their spatiotemporal variability ($r = 0.76$–0.85). Many of the large-scale bromine explosions are successfully reproduced, with the exception of events in May, which are absent or systematically underpredicted in the model. If we assume a lower salinity on MYI (0.01 psu), some of the bromine explosions events observed over MYI are not captured, suggesting that blowing snow over MYI is an important source of bromine activation. We find that the modeled atmospheric deposition onto snow-covered sea ice becomes highly enriched in bromide, increasing from enrichment factors of ~ 5 in September–February to 10–60 in May, consistent with composition observations of freshly fallen snow. We propose that this progressive enrichment in deposition could enable blowing-snow-induced halogen activation to propagate into May and might explain our late-spring underestimate in VCD_{tropo}. We estimate that the atmospheric deposition of SSA could increase snow salinity by up to 0.04 psu between February and April, which could be an important source of salinity for surface snow on MYI as well as FYI covered by deep snowpack. Inclusion of halogen release from blowing-snow SSA in our simulations decreases monthly mean Arctic surface O_3 by 4–8 ppbv (15 %–30 %) in March and 8–14 ppbv (30 %–40 %) in April. We reproduce a transport event of depleted O_3 Arctic air down to 40° N observed at many sub-Arctic surface sites in early April 2007. While our simulation captures 25 %–40 % of the ODEs observed at coastal Arctic surface sites, it underestimates the magnitude of many of these events and entirely misses 60 %–75 % of ODEs. This difficulty in reproducing observed surface ODEs could be related to the coarse horizontal resolution of the model, the known biases in simulating Arctic boundary layer exchange processes, the lack of detailed chlorine chemistry, and/or the fact that we did not include direct halogen activation by snowpack chemistry.

1 Introduction

Ozone depletion events (ODEs) are often observed in the springtime Arctic boundary layer (Barrie et al., 1988; Bottenheim et al., 2009, 1986; Bottenheim and Chan, 2006; Halfacre et al., 2014; Koo et al., 2012; Oltmans et al., 2012; Oltmans and Komhyr, 1986). While ODEs occur episodically at coastal Arctic sites, lasting 1–3 d, they are more persistent and widespread over the frozen ocean (e.g., Simpson et al., 2007b, and references therein). These ODEs have been linked to the release of significant levels of bromine radicals, in a phenomenon called bromine explosion (Abbatt et al., 2012; Simpson et al., 2007b). Both ground-based and satellite instruments have reported elevated BrO columns over the Arctic during March and April (Choi et al., 2012, 2018; Hönninger and Platt, 2002; Jones et al., 2009; Liao et al., 2012; Neuman et al., 2010; Peterson et al., 2017; Salawitch et al., 2010; Simpson et al., 2017; Theys et al., 2011; Wagner et al., 2001). In addition to ODEs in surface air during spring, the elevated bromine radicals result in the rapid oxidation of mercury and its deposition to snowpack (Ebinghaus et al., 2002; Schroeder et al., 1998; Steffen et al., 2008), which can have significant impacts on the health of people and wildlife in polar regions (AMAP, 2011).

An autocatalytic cycle involving the heterogeneous release of sea salt bromide (Br^-) via uptake of HOBr was suggested to be the primary cause of bromine explosions and ODEs (Abbatt et al., 2012; Fan and Jacob, 1992; Hausmann and Platt, 1994; Simpson et al., 2007b).

$$HOBr + Br^-_{aq} + H^+_{aq} \longrightarrow H_2O + Br_2 \quad (R1)$$

$$Br_2 + h\nu \longrightarrow 2Br \quad (R2)$$

$$Br + O_3 \longrightarrow BrO + O_2 \quad (R3)$$

$$BrO + HO_2 \longrightarrow HOBr + O_2 \quad (R4)$$

$$Br + CH_2O \longrightarrow HBr + HCO \quad (R5)$$

$$HBr \xrightarrow{\text{aerosol}} Br^-_{aq} + H^+_{aq} \quad (R6)$$

Reaction (R1) is a multiphase reaction, which takes place on acidic aerosols, cloud droplets, and snow grains. This reaction is required for the initial release of bromine to the atmosphere but also maintains high levels of BrO by allowing the fast recycling of Br^- to reactive bromine (Fan and Jacob, 1992; Lehrer et al., 2004). In addition, the heterogeneous reaction of HOBr with sea salt chloride (Cl^-) can release BrCl from the condensed phase (Abbatt et al., 2012).

In the global troposphere, inorganic bromine (Br_y) has three major sources: the debromination of sea salt aerosol (SSA) produced by breaking waves in the open ocean, photolysis and oxidation of bromocarbons, and transport of Br_y from the stratosphere. Release of Br^- from oceanic SSA is estimated to be the largest global source of tropospheric Br_y (Sander et al., 2003; Zhu et al., 2019). Current global models that include these three sources of tropospheric bromine, as well as multiphase reactions such as Reaction (R1), cannot reproduce the observed elevated levels of tropospheric BrO over polar regions during spring (Parrella et al., 2012; Schmidt et al., 2016). Four classes of substrates specific to polar regions have been proposed as a source of Br^- in Reaction (R1): salty snowpack on sea ice and coastal regions (McConnell et al., 1992; Simpson et al., 2005; Toyota et al., 2011), first-year sea ice (Frieß et al., 2004; Nghiem et al., 2012; Wagner et al., 2007), SSA produced from frost flowers (Kaleschke et al., 2004; Rankin et al., 2002), and SSA produced from blowing salty snow (Jones et al., 2009; Yang et al., 2008).

Both laboratory and outdoor chamber experiments have detected Br_2 production when acidified surface saline snow was exposed to sunlight (Pratt et al., 2013; Wren et al., 2013). However, no Br_2 production was detected over sea ice and brine icicles, suggesting that brines and frost flowers on new sea ice surfaces are not a bromine activation source (Pratt et al., 2013). The proposed role of frost flowers as a direct source of SSA is disputed by several field and laboratory experiments showing that frost flowers are difficult to break even under strong wind conditions (e.g., Alvarez-Aviles et al., 2008; Roscoe et al., 2011; Yang et al., 2017).

A number of studies have focused on the role of aerosols, in particular SSA from blowing snow, as a key mechanism to initiate and sustain bromine activation aloft. Yang et al. (2008) proposed blowing-snow SSA, produced after the sublimation of wind-lofted salty snow on sea ice, as a source of BrO. This source is consistent with satellite observations of large-scale BrO column enhancements over Arctic and Antarctic sea ice, which are often associated with high surface wind speeds that can generate blowing-snow events (Begoin et al., 2010; Blechschmidt et al., 2016; Choi et al., 2018; Jones et al., 2009). Using ground-based measurements in coastal Alaska, Frieß et al. (2004) found that periods of enhanced BrO were coincident with an increase in aerosol extinction at higher wind speeds ($> 5\,m\,s^{-1}$), suggesting that halogen activation and/or recycling takes place in situ on SSA aerosol produced by the sublimation of dispersed snow grains or frost flowers. Peterson et al. (2017) and Simpson et al. (2017) reported aircraft observations of the vertical distribution of BrO and aerosol extinction consistent with initial activation on snowpack followed by transport aloft (500–1000 m), where high BrO was sustained by recycling on aerosols. More recently, Frey et al. (2020) and Giordano et al. (2018) reported direct observations of SSA production from blowing snow above sea ice. In particular, Frey et al. (2020) found that the Br^-/Na^+ ratio of blowing-snow SSA observed at 29 m above the ground decreased by a factor of 2–3 relative to observations at 2 m, suggesting rapid Br^- release via Reaction (R1) from blowing-snow SSA.

There are only a few modeling studies which have examined the link between blowing-snow SSA and bromine explosions. In their pioneering study, Yang et al. (2010) implemented the Yang et al. (2008) blowing-snow parameterization in the p-TOMCAT model and presented a comparison

to satellite retrievals of BrO columns from the Global Ozone Monitoring Experiment (GOME) for 2 months. Their evaluation showed qualitative agreement with observations over polar regions for those months. Theys et al. (2011) describe two 3 d case studies over the Arctic and Antarctic, comparing the p-TOMCAT simulation to tropospheric BrO columns from the second Global Ozone Monitoring Experiment (GOME-2). There was qualitative agreement with the location and timing of the two BrO explosion events. However, Theys et al. (2011) note that beyond these case studies there were large discrepancies between the model and observations, reflecting uncertainties in the p-TOMCAT Br^- emissions, such as assumptions about snow salinity and the fraction of Br^- in SSA released to the gas phase. Zhao et al. (2016) used the UM-UKCA (Unified Model coupled to the United Kingdom Chemistry and Aerosols model) chemistry–climate model to simulate a bromine explosion case study initiated by a blowing-snow event and transported to the Canadian high Arctic. While the model reproduced the vertical extent of the BrO plume, it was not as successful at capturing the timing or magnitude of the observed BrO. Choi et al. (2018) demonstrated a strong spatial and temporal correlation between bromine explosions observed by the Ozone Monitoring Instrument (OMI) and blowing-snow SSA as simulated in the GEOS-5 (Goddard Earth Observing System) modeling system. However, their study did not include a simulation of bromine photochemistry.

Here, we use the GEOS-Chem global chemical transport model to further quantify the role played by blowing-snow SSA in springtime Arctic bromine explosions and examine the associated tropospheric O_3 depletion. We systematically evaluate a 3-year GEOS-Chem simulation (2007–2009) via comparisons to satellite retrievals of tropospheric BrO vertical column densities (VCD_{tropo}) from GOME-2 and OMI. We also compare the model to in situ surface observations of O_3 at several Arctic and sub-Arctic sites. Section 2 describes the GEOS-Chem simulations and the observations used in this study. We evaluate the model's capability to reproduce the timing, magnitude, and spatial extent of bromine explosion events observed by GOME-2 and OMI in Sect. 3. In Sect. 4, we examine the impact of blowing-snow SSA on surface O_3. We assess the contribution of atmospheric deposition to surface snow salinity and bromide content in Sect. 5. Conclusions are presented in Sect. 6.

2 Observations and model simulations

2.1 Satellite observations of tropospheric BrO vertical column densities

The second Global Ozone Monitoring Experiment (GOME-2) is a nadir-scanning ultraviolet–visible spectrometer on the METOP-A (Meteorological Operational) satellite, which was launched on 19 October 2006 in a sun-synchronous polar orbit with an Equator crossing time of 09:30 LT (Munro et al., 2006). The GOME-2 spectrometer covers the 240–790 nm wavelength region, with a spectral resolution between 0.26 and 0.51 nm. It has a ground pixel size of 80 km × 40 km and a scanning swath of 1920 km. In this study, we use the daily 2007–2009 GOME-2 VCD_{tropo} retrieved by Theys et al. (2011). Briefly, the VCD_{tropo} values are derived from a residual technique that combines measured slant columns and calculated stratospheric columns, accounting for the impact of clouds, surface reflectivity, and viewing geometry on the measurement sensitivity. The stratospheric BrO contribution is removed using the dynamic climatology based on the BASCOE (Belgian Assimilation System for Chemical ObsErvations) chemical transport model as described in Theys et al. (2009, 2011). The tropospheric slant columns are converted to vertical columns with a tropospheric air mass factor (AMF) assuming different BrO profile shapes depending on surface albedo. For low surface albedo (< 0.5), a Gaussian-shaped BrO profile with a maximum at 6 km is used. For high surface albedo (> 0.5), the assumed tropospheric BrO concentration profile is constant in the first kilometer above the Lambertian surface reflector. For this second case, which characterizes most of the ice- and snow-covered Arctic, there is a high sensitivity to BrO close to the surface and a weak dependence of the tropospheric AMF to the shape of the profile. As in Theys et al. (2011), we only consider retrievals for values of the solar zenith angle (SZA) of less than 80° and cloud fractions below 0.4 for which the pressure difference between the surface and the top of the cloud is less than 400 mbar.

We also use the BrO VCD_{tropo} from the Ozone Monitoring Instrument (OMI) on board the Aura satellite, which was launched on 15 July 2004 in a sun-synchronous polar orbit with a 13:30 LT Equator overpass time (Levelt et al., 2006). OMI is a nadir solar backscatter spectrometer that measures ultraviolet–visible wavelengths (270–500 nm) and has a horizontal resolution of 13 km × 14 km and swath width of 2600 km. Since 2008, the OMI swath coverage has been reduced due to an external obstruction. We use here the daily 2007–2009 VCD_{tropo} values, which were retrieved by Choi et al. (2018) for the months of March and April poleward of 60° N. The total BrO slant column densities are derived from the OMI total BrO (OMBRO) product, by fitting a model function to OMI ultraviolet backscattered radiance at 319–347.5 nm (Choi et al., 2018). The VCD_{tropo} values are retrieved using the same residual technique and dynamic climatology stratospheric BrO columns as in Theys et al. (2011). In the OMI tropospheric AMF calculation, the assumed BrO shape profile is based on a composite of aircraft measurements obtained during the NASA Arctic Research of the Composition of the Troposphere from Aircraft and Satellites (ARCTAS) campaign (Choi et al., 2012). We use the same selection criteria as in Choi et al. (2018) – SZA $< 80°$ and surface reflectivity > 0.6 – and only retain observations with low cloud contamination (difference between OMI rota-

tional Raman cloud pressure and terrain pressure < 100 hPa). The uncertainty of OMI and GOME-2 VCD_{tropo} retrieved over the highly reflective surfaces of polar regions is on the order of 30 %–50 %.

2.2 Surface O_3 measurements

We use hourly in situ O_3 measurements at three Arctic surface sites: Utqiaġvik, Alaska (also known by the former city name and current station name of Barrow; 71.3° N, 156.6° W; 8 m above sea level), from the NOAA Earth System Research Laboratory; Alert, Nunavut (82.5° N, 62.5° W; 187 m), from the Canadian Air and Precipitation Monitoring Network (CAPMoN); and Zeppelin, Spitsbergen (78.9° N, 11.8° E, 474 m), from the Norwegian Institute for Air Research. We also use hourly surface O_3 measurements at several sub-Arctic sites from CAPMoN as well as from the Canadian National Air Pollution Surveillance (NAPS) network and from the United States Clean Air Status and Trends Network (CASTNET). For the NAPS sites, we only consider sites sampling background air in the categories "forest" and "undeveloped rural", and for CASTNET we exclude sites located in "urban/agricultural" areas. This selection allows us to avoid more polluted sites, which can be subject to low winter–spring O_3 concentrations associated with the NO titration of O_3. The sub-Arctic sites include Bonner Lake (49.4° N, 82.1° W; 242 m), Algoma (47.0° N, 84.38° W; 411 m), and Egbert (44.2° N, 79.8° W; 206 m) from the CAPMoN network, as well as Elk Island (53.68° N, 112.87° W; 714 m) from NAPS and Woodstock (43.94° N, 71.70° W; 255 m) from CASTNET.

2.3 The GEOS-Chem chemical transport model

GEOS-Chem is a three-dimensional global chemical transport model (Bey et al., 2001). In this work, we use GEOS-Chem v11-02d (http://www.geos-chem.org, last access: 19 August 2019), driven by the Modern-Era Retrospective analysis for Research and Applications, version 2 (MERRA-2) assimilated meteorological fields (Gelaro et al., 2017), which have a native horizontal resolution of 0.5° latitude by 0.625° longitude with 72 vertical levels. We regrid the MERRA-2 fields to a 2° × 2.5° horizontal resolution and 47 vertical levels with merged levels above 80 hPa for computational expediency. For the time period of the simulations conducted here (2007–2009), the daily boundary conditions for sea ice concentrations in MERRA-2 are from the high-resolution (1/20°) Operational SST (sea surface temperature) and Sea Ice Analysis (OSTIA), which uses daily sea ice concentration products from multiple Special Sensor Microwave Imager (SSM/I) satellites (Donlon et al., 2012).

Global anthropogenic emissions are from EDGAR v4.2 (Emissions Database for Global Atmospheric Research; Olivier and Berdowski, 2001) for 1970–2008. Biomass burning emissions are from the Global Fire Emissions Database version 4 (GFEDv4) emission inventory (van der Werf et al., 2017). Biogenic emissions of volatile organic compounds (VOCs) are from the Model of Emissions of Gases and Aerosols from Nature version 2.1 (MEGAN 2.1) (Guenther et al., 2012).

GEOS-Chem simulates detailed HO_x–NO_x–VOC–O_3–halogen–aerosol tropospheric chemistry. The chemical mechanism in GEOS-Chem v11-2d was updated to the most recent recommendations of the Jet Propulsion Laboratory (JPL) and the International Union of Pure and Applied Chemistry (IUPAC) as described in Fischer et al. (2014, 2016), Mao et al. (2013), and Travis et al. (2016). This version of GEOS-Chem includes bromine–chlorine–iodine halogen chemistry. The bromine chemistry mechanism was first described in Parrella et al. (2012). The mechanism was then updated by Schmidt et al. (2016) to include extensive multiphase chemistry as well as coupling to tropospheric chlorine chemistry, which provides an important pathway to recycle bromine radicals. The uptake coefficients for the heterogeneous reactions of HOBr, $ClNO_3$, and O_3 with Br^- in aerosols, as well as for the reaction of HOBr with Cl^- in aerosols, follow Ammann et al. (2013). The uptake coefficient between O_3 and Br^- considers both bulk and surface reactions. Sherwen et al. (2016a, b) implemented iodine chemistry and Cl-Br-I interactions. Chen et al. (2017) added the in-cloud oxidation of dissolved SO_2 (S(IV)) by HOBr in GEOS-Chem, which decreased the global Br_y burden by 50 % and resulted in improved agreement with GOME-2 VCD_{tropo} between 60° N and 60° S. A total of 15 bromine tracers are transported (Br_2, Br, BrO, HOBr, HBr, $BrNO_2$, BrCl, $BrONO_2$, $CHBr_3$, CH_2Br_2, CH_3Br, IBr, CH_2IBr, Br^- on accumulation mode SSA, and Br^- on coarse-mode SSA), with sources from the photolysis of $CHBr_3$; the oxidation of $CHBr_3$, CH_2Br_2, and CH_3Br by OH radicals; the transport of reactive bromine from the stratosphere; and SSA debromination driven by explicit heterogeneous reactions of SSA Br^- with HOBr, $ClNO_3$, and O_3.

Open-ocean emissions of SSA are a function of wind speed and sea surface temperature (SST) as described in Jaeglé et al. (2011), with updates from Huang and Jaeglé (2017) for cold ocean waters (SST < 5 °C). Two separate SSA tracers are transported: accumulation mode SSA (r_{dry} = 0.01–0.5 µm) and coarse-mode SSA (r_{dry} = 0.5–8 µm). Sea salt Br^- is emitted assuming a ratio of 2.11×10^{-3} kg Br per kg dry SSA, based on the composition of sea water (Lewis and Schwartz, 2004; Sander et al., 2003). Sea salt Br^- is transported in two tracers as part of accumulation mode and coarse-mode SSA.

The blowing-snow SSA simulation in GEOS-Chem

The blowing-snow SSA simulation in GEOS-Chem is described in Huang and Jaeglé (2017) and Huang et al. (2018). Blowing-snow SSA emissions are a function of relative humidity, temperature, the age of the snow, surface snow salin-

ity, and wind speed following the parameterization of Yang et al. (2008, 2010). As in Huang and Jaeglé (2017), we assume $N = 5$ for the number of SSA particles produced per snowflake and a mean snow age of 3 d over the Arctic. Two key parameters controlling the magnitude of blowing-snow SSA production and subsequent heterogeneous Br^- release are the surface snow salinity and Br^- content, both of which have very few observational constraints. Sea salt and Br^- in surface snow originate from the upward migration of brine from sea ice, the atmospheric deposition of SSA as well as gas-phase reactive bromine species, and the contamination of snow by frost flowers (Abbatt et al., 2012). Domine et al. (2004) estimate that frost flowers could account for 10 % of the observed surface snow salinity. The upward migration of brine is expected to be the dominant source of salinity for thin snow over sea ice (< 10–17 cm; Domine et al., 2004; Peterson et al., 2019). As the snow depth gets thicker, the salinity of surface snow decreases and the influence of atmospheric deposition likely becomes more important (Krnavek et al., 2012; Nandan et al., 2017). Snow over first-year sea ice (FYI) is typically more saline than over multi-year sea ice (MYI), as MYI is desalinated by flushing and gravity drainage during repeated summer melt cycles.

Krnavek et al. (2012) sampled the chemical composition of surface snow on land-fast sea ice near Utqiaġvik, Alaska. They reported a median salinity of 0.7 practical salinity unit (psu) for 2–3-week-old FYI, 0.1 psu for thicker FYI, and 0.01 psu for MYI. Domine et al. (2004) reported a salinity of 0.02 psu for MYI near Alert. Peterson et al. (2019) measured surface snow in FYI and MYI regions near Greenland, Alaska, and in the central Arctic, finding higher mean salinities for snowpacks less than 17 cm deep (0.15 psu) compared to deeper snowpacks (0.02 psu). The observed Br^- concentrations in surface snow over Arctic sea ice is highly variable, ranging from 10^{-2} to 10^3 µM (Domine et al., 2004; Krnavek et al., 2012; Peterson et al., 2019). This high variability is accompanied with either depletion or enhancement in the bromide-to-sodium (Br^-/Na^+) ratio relative to sea water composition. Depletion in Br^- relative to seawater indicates loss to the atmosphere via heterogeneous reactions. Enhancements can be the result of precipitation of hydrohalite ($NaCl\text{-}2H_2O$) below 251 K in brine (Koop et al., 2000; Morin et al., 2008). Indeed, the laboratory measurements of aqueous NaCl and sea salt solution droplets of Koop et al. (2000) show a factor of 12 increase in the Br^-/Na^+ ratio at 240 K relative to 273 K. Enhancements in Br^- could also be caused by the deposition of atmospheric aerosol and HBr produced during bromine explosions onto surface snow (Simpson et al., 2005, 2007b). Domine et al. (2004) report measurements of surface snow on sea ice near Alert, with a factor of 5 enrichment in Br^- relative to seawater, while surface snow over an Arctic Ocean site further north displayed a Br^- enrichment of 25. Samples of surface snow on MYI appear to be enhanced in Br^- more often than on FYI (Krnavek et al., 2012), which suggests that MYI, in addition to FYI, could play an active role in Arctic boundary layer bromine and chlorine chemistry (Peterson et al., 2019).

We conduct three GEOS-Chem simulations as part of this work: a standard simulation (referred to as "STD"), in which the only source of SSA is from the open ocean, and two simulations in which we add a blowing-snow source of SSA. In the first blowing-snow simulation (referred to as "FYI Snow"), we assume an Arctic surface snow salinity of 0.1 psu on FYI and 0.01 psu on MYI. In the second blowing-snow simulation ("FYI+MYI Snow"), we use a salinity of 0.1 psu on FYI and 0.05 psu on MYI. These two salinities assumed for MYI are used to examine the role of bromine activation on MYI. For both blowing-snow simulations, we assume a surface snow Br^- enrichment factor of 5 relative to sea water (sea salt Br^- is emitted, assuming a ratio of 10.55×10^{-3} kg Br per kg dry blowing-snow SSA emitted). As sea ice age is not tracked in MERRA-2, for each year we identify the location of Arctic MYI from the preceding September minimum sea ice extent in MERRA-2. The FYI extent is calculated by subtracting the MYI extent from the total sea ice extent. Note that this very simple approach does not account for the advection and melting of MYI between one September to the next. All simulations are initialized with a 6-month spin-up in 2006 and then followed by a 3-year simulation for 2007–2009.

In previous work (Huang et al., 2018; Huang and Jaeglé, 2017), we found that the GEOS-Chem blowing-snow simulation (using 0.1 psu on FYI and 0.01–0.1 psu on MYI) reproduced the seasonal cycle and magnitude of SSA mass concentrations observed at Utqiaġvik, Alert, and Zeppelin but that the STD simulation underestimates observations by a factor of 2–10 during winter and spring. The blowing-snow simulations also reproduced the seasonal cycle of aerosol extinction coefficients observed in the lower troposphere (0–2 km) over Arctic sea ice by the Cloud-Aerosol Lidar with Orthogonal Polarization (CALIOP) on board the CALIPSO satellite (Huang et al., 2018).

For comparison with satellite retrievals of VCD_{tropo}, we sample the model at 09:00–11:00 LT, which corresponds to the overpass times of GOME-2 in the Northern Hemisphere. We found that sampling GEOS-Chem at 13:00–15:00 LT, matching the OMI overpass time, results in less than a 1 % difference in VCD_{tropo}. We thus only show the model results for 09:00–11:00 LT. We regrid daily OMI and GOME-2 VCD_{tropo} to a horizontal resolution of $2° \times 2.5°$ for comparison to GEOS-Chem. The model is sampled on days and locations of GOME-2 and OMI with available retrievals.

3 Evaluation of the impact of blowing-snow SSA on BrO VCD_{tropo}

3.1 Seasonal cycle of VCD_{tropo} in the Northern Hemisphere

Several previous GEOS-Chem model versions have been evaluated against GOME-2 BrO VCD_{tropo}. Schmidt et al. (2016) showed that the inclusion of SSA debromination resulted in a 50 %–100 % overestimate in BrO in the Northern Hemisphere. Sherwen et al. (2016a, b) added iodine chemistry and disabled SSA debromination, finding relatively good agreement with GOME-2 observations over the Arctic and the summertime low latitudes and midlatitudes. Chen et al. (2017) enabled SSA debromination and added the in-cloud oxidation of dissolved S(IV) with HOBr to the model version of Schmidt et al. (2016) without iodine chemistry. They found improved agreement with GOME-2 VCD_{tropo} over low latitudes and midlatitudes but underestimations by a factor of 3–10 over high latitudes. Our STD simulation includes SSA debromination; the in-cloud oxidation of dissolved S(IV) by HOBr, as well as iodine chemistry; and chlorine chemistry.

Figure 1a and b shows that with these four components, the STD simulation agrees well with the GOME-2 VCD_{tropo} at 0–30 and 30–60° N averaged for 2007–2009. Over the Arctic (> 60° N), however, the STD simulation underestimates GOME-2 and OMI observations by up to 50 % during spring (Fig. 1c). Note that we do not show monthly mean GOME-2 VCD_{tropo} at 60–90° N for November–February, as less than 70 % of the polar region has valid data (SZA is generally greater than 80° for these months).

The 2007–2009 GOME-2 and OMI VCD_{tropo} values display a March–April maximum of ~ 3–3.5×10^{13} molecules cm^{-2} poleward of 60° N (Fig. 1c). The inclusion of blowing-snow SSA emissions in the GEOS-Chem FYI Snow simulation increases the modeled springtime VCD_{tropo} by 42 % in March and 52 % in April, improving the agreement with satellite retrievals (Fig. 1c). The FYI+MYI Snow simulation increases the modeled VCD_{tropo} by another 10 %–20 % in March and April. Both blowing-snow simulations are within 5 %–20 % of the observed VCD_{tropo} values in March and April; however they predict too rapid of a decrease in VCD_{tropo} in May.

In late summer and fall, when sea ice extent is at its minimum and blowing-snow SSA emissions are negligible, GEOS-Chem underestimates GOME-2 VCD_{tropo} by 30 %–40 %. Over the cloudy summer Arctic, the reaction HOBr + S(IV) in cloud water provides a sink for HOBr and decreases the Br_y abundance by about 70 %–90 % (Chen et al., 2017). We hypothesize that including acid displacement HCl from SSA would lead to an increase in HOBr because of the competition between $HOBr + Cl^-$ (which recycles HOBr by producing BrCl) and HOBr + S(IV) (which is a sink for HOBr) in cloud droplets. Indeed, in a subsequent version of GEOS-Chem, X. Wang et al. (2019) added this source of HCl, finding an increase in BrO, especially in cloudy high latitudes.

3.2 Spatial distribution of springtime Arctic BrO VCD_{tropo}

Figure 2 shows the spatial distribution of monthly mean VCD_{tropo} during March and April 2007–2009. In March, both GOME-2 and OMI exhibit enhanced VCD_{tropo} (3.5–5×10^{13} molecules cm^{-2}) in an arc between Baffin Bay – along the west coast of Greenland – and the Laptev Sea – off the northern coast of Siberia. In April, the observed VCD_{tropo} reach values > 3.5–4×10^{13} molecules cm^{-2} over most of the sea-ice-covered Arctic Ocean. Figure 3a compares the GOME-2 and OMI VCD_{tropo} poleward of 60° N for March and April 2007–2009, showing that they are highly correlated ($r = 0.92$, slope = 0.99), with OMI being 13 % higher than GOME-2.

As shown in Figs. 2 and 3d, the GEOS-Chem STD simulation predicts VCD_{tropo} lower than 2.5–3×10^{13} molecules cm^{-2} in March–April, with little spatial variability compared to observations ($r = 0.22$–0.36). The normalized mean bias ($NMB = 100 \times \sum(M_i - O_i)/\sum O_i$, with observations O_i and model M_i summed poleward of 60° N) is −41 % compared to OMI and −34 % compared to GOME-2. The FYI Snow simulation has more success at reproducing the magnitude of the observed VCD_{tropo} in March and April (NMB = −12 % relative to OMI and NMB = +1 % relative to GOME-2), as well as their spatial distribution ($r = 0.70$–0.76). The VCD_{tropo} values predicted by the FYI+MYI Snow simulation agree better with OMI (NMB = +2 % and $r = 0.76$) but overestimate GOME-2 (NMB = +17 % and $r = 0.79$). Similar to the satellite retrievals in March, the FYI Snow and FYI+MYI Snow simulations display the largest VCD_{tropo} over the Canadian Arctic Archipelago (Fig. 2), with secondary maxima over Baffin Bay, the Greenland Sea, and the East Siberian Sea. In April, the VCD_{tropo} in the FYI Snow simulation underestimates GOME-2 and OMI throughout the Arctic, but the FYI+MYI Snow simulation overestimates satellite observations in the high Arctic (> 80° N), while underestimating observations at 70–80° N. This suggests spatial variability in salinity and/or Br^- enhancement for snow that is not captured in our assumptions of spatially uniform values for FYI and MYI. We also find that the simulated VCD_{tropo} values underestimate observations over the coastal Arctic, especially in April. This could be due halogen activation from snow over land (Simpson et al., 2005), which is not considered in our simulation, as we assume zero salinity and Br^- content in continental snow.

3.3 Daily variations in pan-Arctic BrO VCD_{tropo}

Figure 4a shows that GOME-2 daily mean VCD_{tropo} values poleward of 60° N are highest in March–April and then decrease in May. The OMI VCD_{tropo} values in March and

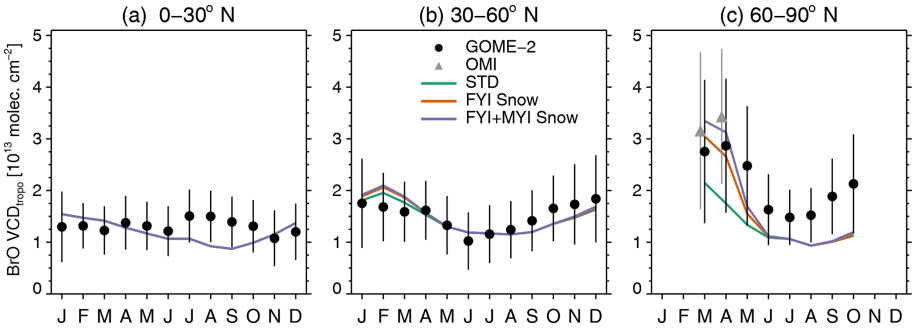

Figure 1. Seasonal variation in 2007–2009 monthly mean tropospheric BrO vertical column densities (VCD_{tropo} in units of 10^{13} molecules cm^{-2}) observed by GOME-2 (black circles) and OMI (gray triangles in panel **c** for April and May) and simulated with GEOS-Chem over **(a)** 0–30° N, **(b)** 30–60° N, and **(c)** 60–90° N. The three GEOS-Chem simulations shown are the standard simulation (STD, green line) and two blowing-snow simulations (FYI Snow, orange line, and FYI+MYI Snow, purple line). The black and gray error bars represent 1 standard deviation about the monthly mean GOME-2 and OMI VCD_{tropo}. For each latitude bin, we only show means for months where at least 70 % of the surface area has valid satellite observations.

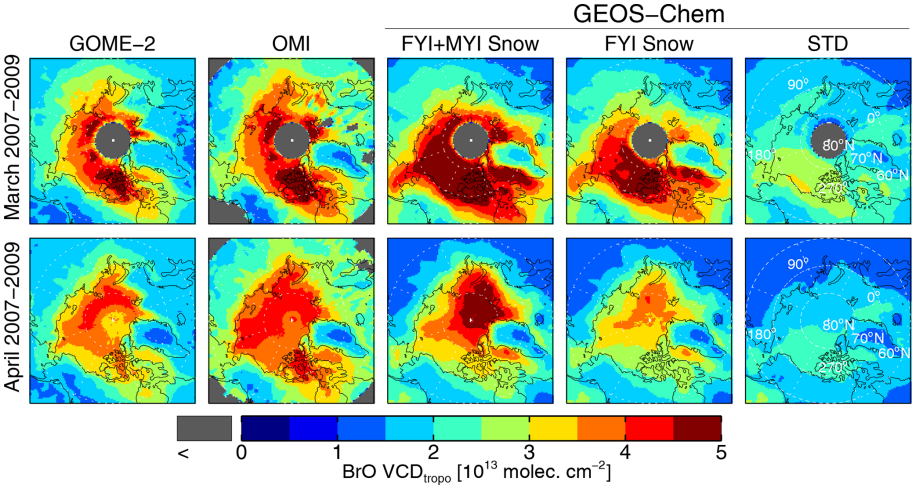

Figure 2. Spatial distribution of VCD_{tropo} in March (top row) and April (bottom row) 2007–2009. Satellite retrievals from GOME-2 and OMI are compared to the GEOS-Chem FYI+MYI Snow, FYI Snow, and STD simulations.

April display a similar day-to-day variability as GOME-2 observations. Overall the FYI+MYI Snow simulation shows good agreement with the magnitude and daily variability of the combined mean GOME-2 and OMI VCD_{tropo} (NMB = −8.3 %, $r = 0.85$). While the FYI+MYI Snow simulation reproduces the March–April VCD_{tropo}, it predicts too rapid of a decrease in May for all 3 years (Fig. 4a). The difference between the FYI Snow and MYI+FYI Snow simulations is the largest in April as polar sunrise reaches the high Arctic, where the majority of MYI is located. Most of the BrO enhancements in the two blowing-snow simulations occur below 1 km altitude, occasionally extending to 2 km (see Fig. S1a and b in the Supplement).

As discussed in previous studies (Choi et al., 2018; Nghiem et al., 2012; Richter et al., 1998; Salawitch et al., 2010; Theys et al., 2011) satellite observations show the frequent occurrence of "BrO hotspots" over Arctic sea ice during spring. For this study, we define a BrO hotspot when local VCD_{tropo} values exceed 4.5×10^{13} molecules cm^{-2}, which is the 90th percentile of GOME-2 VCD_{tropo} poleward of 60° N in March–April. For OMI, the corresponding 90th percentile is 5.1×10^{13} molecules cm^{-2}. We use these respective criteria to calculate the daily area covered by BrO hotspots as observed by GOME-2 and OMI. The episodic nature of GOME-2 and OMI BrO hotspots is apparent in Fig. 4b, which shows a large degree of daily variability, with events lasting between a few days and 2 weeks. The light-orange shading in Fig. 4 identifies multi-day events (> 5 d) when the GOME-2 hotspot area exceeds 2×10^6 km^2. There are two such events in both 2007 and 2008 and three events in 2009 (Fig. 4b). These events reach maximum extents of 4–6×10^6 km^2. For comparison, the mean sea ice extent during March–April poleward of 60° N is $\sim 10 \times 10^6$ km^2 (with a split of ∼ 65 % to 35 % between FYI and MYI).

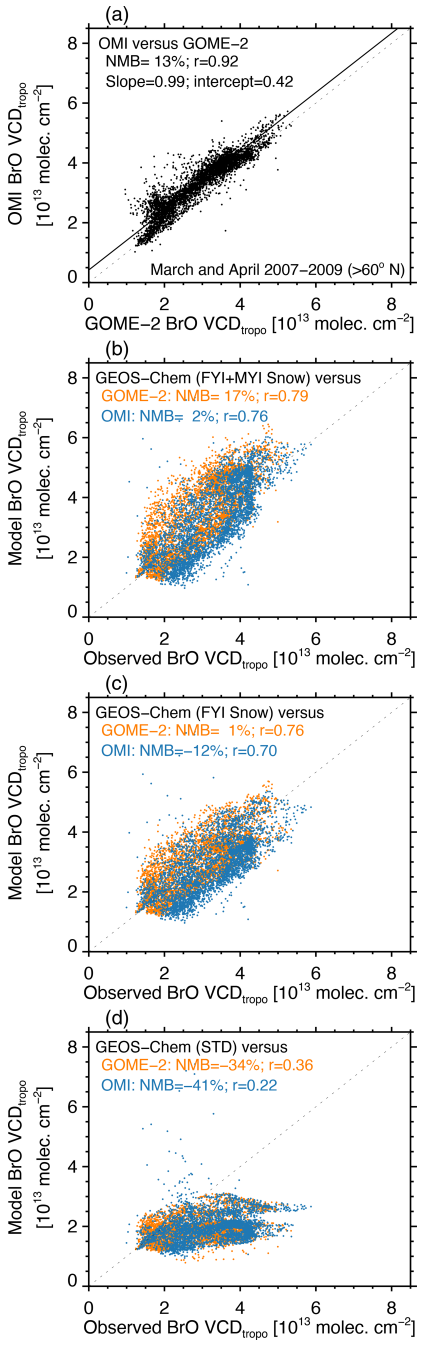

Figure 3. **(a)** Scatterplot of GOME-2 and OMI monthly mean VCD_{tropo} for March and April 2007–2009 poleward of 60° N. **(b)** Scatterplot of VCD_{tropo} calculated with the FYI+MYI Snow simulation and retrieved by GOME-2 (orange circles) and OMI (blue circles). **(c)** Same as panel **(b)** but for the FYI Snow simulation. **(d)** Same as panel **(b)** but for the STD simulation. The normalized mean bias (NMB; see definition in Sect. 3.1), Pearson correlation coefficient, and slope are shown in each panel. For panel **(b)**, the slope and intercept of the reduced-major-axis regression line (solid line) are also indicated. The dashed line corresponds to the 1 : 1 line.

We apply the OMI threshold ($VCD_{tropo} > 5.1 \times 10^{13}$ molecules cm^{-2}) to the GEOS-Chem simulations. On average, the FYI+MYI Snow simulation reproduces the observed spatial extent of BrO hotspots to within 4 % and captures the timing of the two large-scale episodes in 2007 (26 March–4 May and 10–20 May 2007) and the two episodes in 2008 (7–17 March and 1–8 April 2008). For 2009, the FYI+MYI Snow simulation predicts two episodes (5–15 March and 11–23 April), but the aerial extent of these episodes is overestimated, and the simulation misses the third episode on 6–19 May 2009 (Fig. 4b). In the model, the variability in BrO hotspots is driven by the temporal variations of the blowing-snow SSA burden (Fig. 4c).

3.4 Two case studies of large BrO explosion events

Figure 5 shows the daily spatial distribution of VCD_{tropo} on 25–30 March 2007, corresponding the largest BrO hotspot episode observed by GOME-2 and OMI during our study period (Fig. 4a and b). The GOME-2 and OMI VCD_{tropo} exceed 7×10^{13} molecules cm^{-2} (up to 15×10^{13} molecules cm^{-2}) over the sea-ice-covered region in the high Arctic region (> 70° N). The enhanced VCD_{tropo} occurrences start on 25 March over the East Siberian Sea and then rotate counterclockwise, reaching the Beaufort Sea on 27 March and the Canadian Arctic Archipelago on 28–30 March 2007. This event was previously discussed in Begoin et al. (2010) and Choi et al. (2018). Begoin et al. (2010) used the FLEXPART (FLEXible PARTicle) particle dispersion model to link the enhanced GOME-2 VCD_{tropo} to a cyclone with very high surface wind speeds, favorable for generating blowing-snow SSA. Choi et al. (2018) found that the spatial pattern of OMI VCD_{tropo} was consistent with that of the GEOS-5 simulated blowing-snow SSA burden on both FYI and MYI, while restricting the blowing-snow emissions to FYI only did not agree as well with the observed VCD_{tropo}. Our FYI+MYI Snow simulation reproduces the evolution of this BrO hotspot, although the magnitude of the modeled VCD_{tropo} overestimates observations after 28 March 2007. The main difference between the FYI Snow and FYI+MYI Snow simulations is on 25–26 March 2007, when the high winds are located over the North Pole, where MYI is found (Figs. 5 and S2). As there are no valid GOME-2 and OMI retrievals at these high latitudes (SZA > 80°), we cannot assess which simulation agrees better with observations for this case study.

Figure 6 shows the daily distribution of VCD_{tropo} on 14–19 April 2007. During this event, there is a factor of 1.5 difference in pan-Arctic VCD_{tropo} calculated with the FYI Snow and FYI+MYI Snow simulations (Fig. 4a). The GOME-2 and OMI VCD_{tropo} show high values ($> 5 \times 10^{13}$ molecules cm^{-2}) being maintained over the North Pole (Fig. 6). The MERRA-2 meteorological fields predict high surface winds (> 10–12 m s^{-1}) in that area, which is covered by MYI (Fig. 7, bottom row). The VCD_{tropo} values calcu-

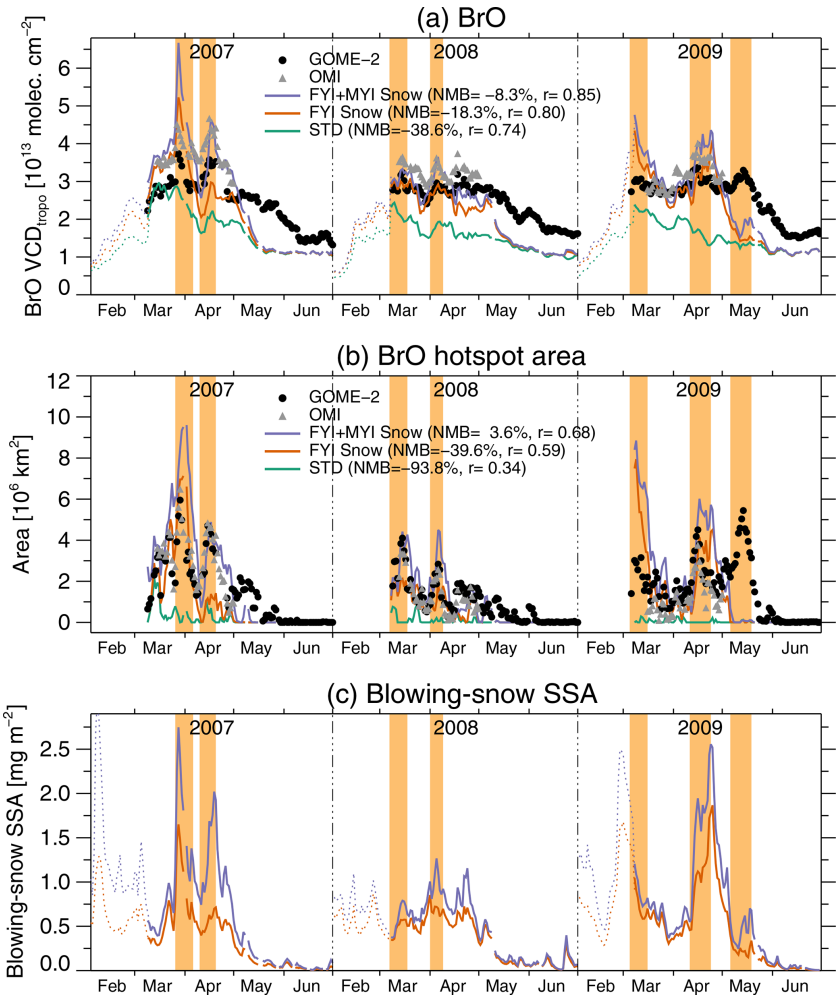

Figure 4. Time series of daily mean BrO VCD$_{tropo}$, tropospheric BrO hotspots area, and blowing-snow SSA burden over high latitudes (> 60° N) between February and June for 2007–2009. **(a)** Time series of daily VCD$_{tropo}$ (in 10^{13} molecules cm^{-2}) averaged poleward of 60° N for GOME-2 (black circles) and OMI (gray triangles) and simulated with GEOS-Chem (FYI+MYI Snow, purple; FYI Snow, orange; and STD, green). **(b)** The daily area extent of BrO hotspots (in units of 10^6 km^2) for GOME-2, OMI, and GEOS-Chem. See Sect. 3.3 for the definition of BrO hotspot areas. Note that the total area poleward of 60° N is 34.2×10^6 km^2. **(c)** Time series of the daily mean blowing-snow SSA burden (mg m^{-2}) for the FYI+MYI Snow and FYI Snow simulations. The blowing-snow SSA burden is obtained as the difference between the blowing-snow and STD simulations. The normalized mean bias (NMB) and Pearson correlation coefficients displayed in panels **(a)** and **(b)** are relative to the combined GOME-2 and OMI time series. The events highlighted in light orange are defined as periods when GOME-2 or OMI BrO hotspots cover more than 2×10^6 km^2 for longer than 5 d. We only show days where valid satellite observations are available over at least 70 % of the surface area poleward of 60° N. The dashed lines in panels **(a)** and **(c)** correspond to the GEOS-Chem daily means poleward of 60° N for days with less than 70 % of valid observations.

lated by the FYI Snow simulation show little enhancement over the North Pole (Fig. 7), while the FYI+MYI Snow simulation better captures the magnitude and shape of the observed enhancement (Fig. 6), suggesting that blowing-snow SSA emissions over MYI can be a significant source of BrO.

Overall, we find that the FYI+MYI Snow simulation captures reasonably well the spatial and temporal distribution of the observed VCD$_{tropo}$, as well as the spatial extent and frequency of BrO hotspots in March and April. In our simulation, blowing-snow SSA emissions on MYI account for 20 %–30 % of the VCD$_{tropo}$ enhancement and could thus represent an important source of bromine activation. This is consistent with previous studies, which have suggested that, in addition to FYI, MYI could play a significant role in halogen activation. Gilman et al. (2010) used back trajectories to calculate sea ice exposure of air masses observed during the International Chemistry Experiment in the Arctic Lower Troposphere (ICEALOT) ship-based study, finding that exposure to both FYI and MYI was the best predictor of reduced O_3 levels. Choi et al. (2018) reported that the frequency of

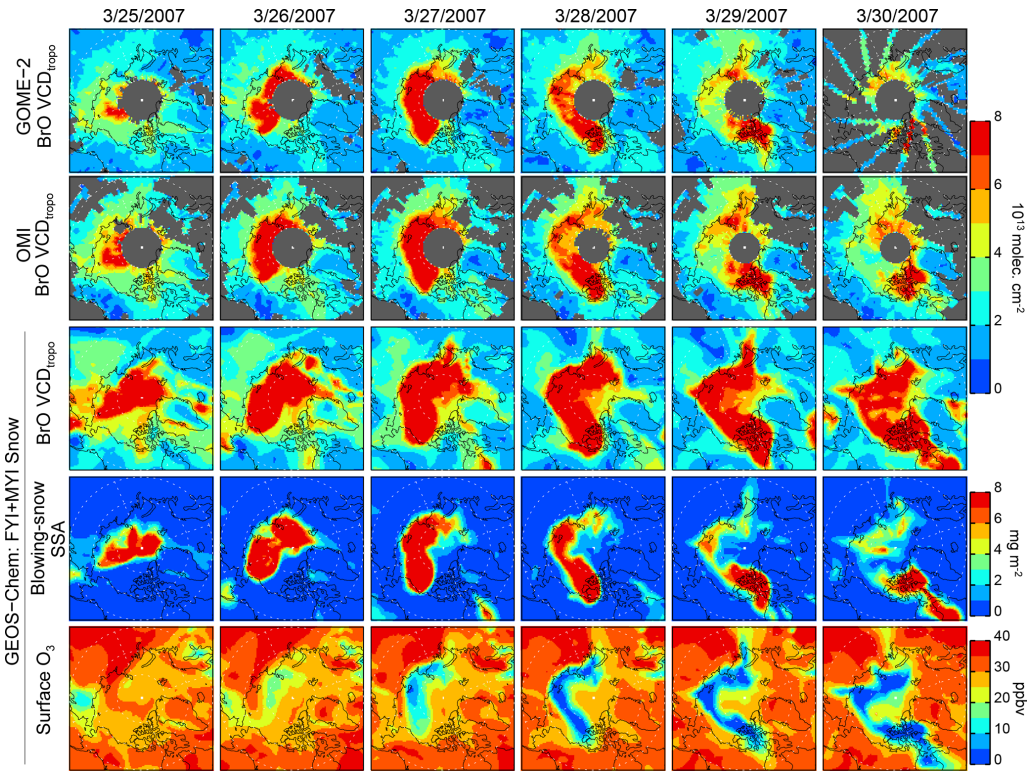

Figure 5. Daily 25–30 March 2007 (in the date format of month/day/year) distribution of BrO VCD_{tropo} for GOME-2, OMI, and GEOS-Chem (FYI+MYI Snow simulation). Also shown are the blowing-snow SSA mass burdens (mg m^{-2}) and surface O_3 mixing ratios (ppbv) for the FYI+MYI Snow simulation. The gray areas in the first two rows correspond to regions with no BrO retrievals. Note that polar sunrise occurred equatorward of 80° N.

springtime BrO explosion events observed by OMI for 2005–2015 was strongly correlated with blowing-snow SSA emissions over all sea ice, but they found little-to-no correlation when only FYI was considered as a source of blowing-snow SSA. Rhodes et al. (2017) found that simulations including blowing-snow SSA emissions on MYI had better skill at reproducing surface observations of SSA in the Arctic compared to simulations without SSA emissions on MYI. More generally, low O_3 and/or high BrO VCD_{tropo} values have been observed over and downwind of regions with a high fraction of MYI such as the Canadian Arctic Archipelago and the eastern Beaufort Sea (Bottenheim and Chan, 2006; Choi et al., 2012; Halfacre et al., 2014; Koo et al., 2012; Richter et al., 1998; Salawitch et al., 2010). In contrast to the generally good agreement in March and April, during May our simulation is systematically too low compared to GOME-2 VCD_{tropo} (Figs. 1c and 4a, b). In Sect. 5 we will discuss how the recycling of bromine deposition to snowpack in late spring could propagate blowing-snow-induced halogen activation into May.

4 Impact of blowing-snow SSA on tropospheric O_3 over the Arctic

4.1 Comparison to hourly surface O_3 observations

We evaluate the ability of our simulations to capture ODEs via comparisons to hourly O_3 observations at several Arctic and sub-Arctic sites for 1 March–31 May 2007 (Fig. 8). Observations at Utqiaġvik and Alert show frequent occurrences of low O_3 mixing ratios (< 10 ppbv), maintained for 1–7 d. These events are somewhat less frequent at Zeppelin. Figure 8 shows that FYI+MYI Snow simulation reproduces only 25 %–30 % of the ODEs at Utqiaġvik and Alert, such as the 8–18 April and 26 April–10 May depletion events at Utqiaġvik as well as the April events at Alert. The model-predicted magnitude of O_3 depletion at those sites is a factor of 2 lower than the observed values. The FYI+MYI Snow simulation performs somewhat better at Zeppelin, where it captures the timing and magnitude of 40 % of the observed events, in particular between late March and late April. Our simulation thus misses 60 %–75 % of observed ODEs at those three Arctic sites, including several events in March and late May at Utqiaġvik, as well as the sustained May events at Alert, and the ODEs in late May at Zeppelin.

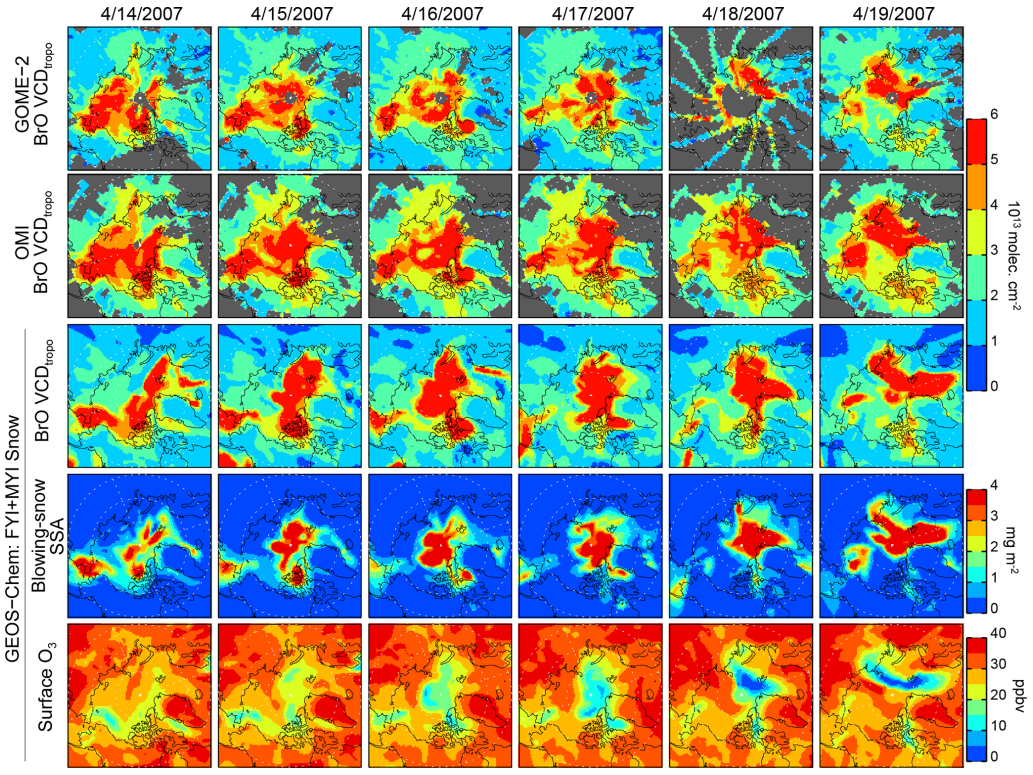

Figure 6. Daily 14–19 April 2007 (in the date format of month/day/year) distribution of BrO VCD_{tropo} from GOME-2, OMI, and GEOS-Chem (FYI+MYI Snow simulation). Also shown are the blowing-snow SSA burdens (mg m^{-2}) and surface O_3 mixing ratios (ppbv) in the FYI+MYI Snow simulation.

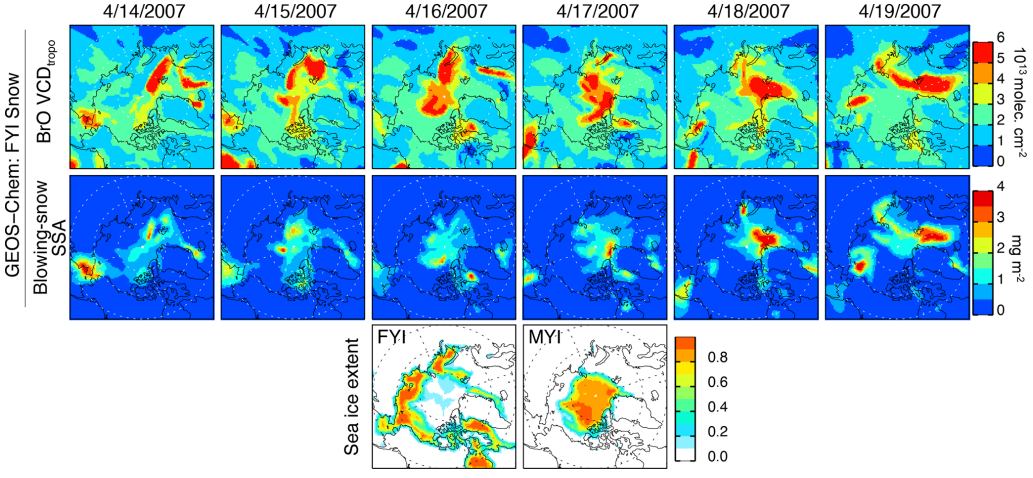

Figure 7. Daily 14–19 April 2007 (in the date format of month/day/year) distribution of BrO VCD_{tropo} and blowing-snow SSA burden from the GEOS-Chem FYI Snow simulation. The bottom row shows the distribution of sea ice extent for FYI and MYI.

Observed surface O_3 depletion events can be caused by the advection of upwind O_3 poor air and/or local depletion (Bottenheim and Chan, 2006; Halfacre et al., 2014; Hopper et al., 1998; Jacobi et al., 2006; Simpson et al., 2007b, 2017). The rapid recovery of surface O_3 after a depletion event is often due to the turbulent vertical mixing of O_3-rich free-tropospheric air down to the surface or to the advection of O_3-rich continental air (Bottenheim et al., 2009; Gong et al., 1997; Hopper et al., 1998; Jacobi et al., 2010; Moore et al., 2014; Morin et al., 2005). Furthermore, some ODEs can be highly localized. Using ice-tethered buoys over coastal regions and over the Arctic Ocean, Halfacre et al. (2014) found that large areas of the Arctic Ocean are partially depleted in O_3 during spring with local imbedded areas ($\sim$ 200–300 km)

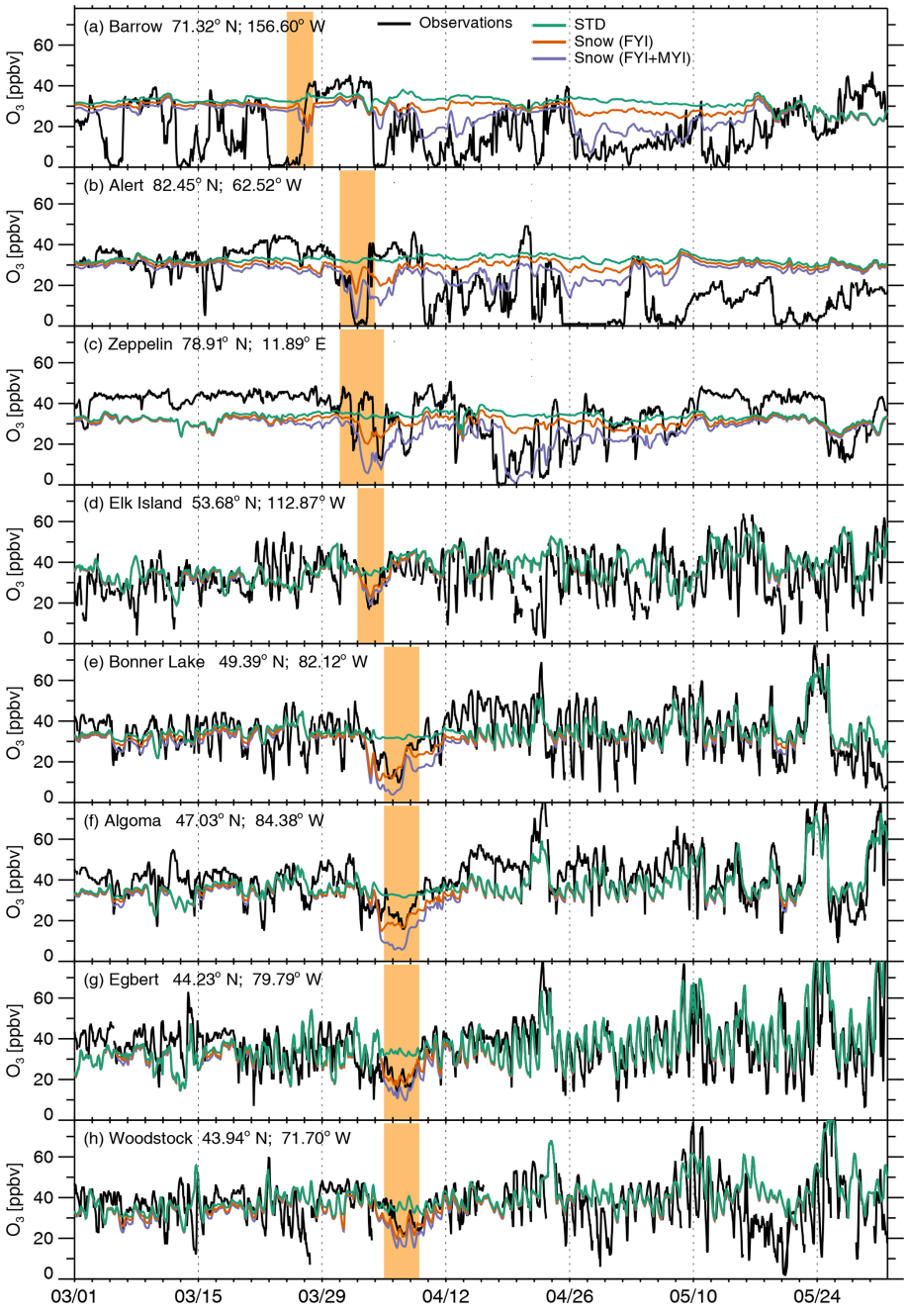

Figure 8. Time series of hourly surface O_3 (ppbv) at three Arctic sites **(a–c)** and five sub-Arctic sites **(d–h)** for 1 March–31 May 2007 (in the date format of month/day): **(a)** Utqiaġvik (Barrow), Alaska, USA; **(b)** Alert, Nunavut, Canada; **(c)** Zeppelin, Spitsbergen, Norway; **(d)** Elk Island, Alberta, Canada; **(e)** Bonner Lake, Ontario, Canada; **(f)** Algoma, Ontario, Canada; **(g)** Egbert, Ontario, Canada; and **(h)** Woodstock, New Hampshire, USA. In situ observations are shown with the black lines, while the GEOS-Chem STD, FYI Snow, and FYI+MYI Snow simulations are shown in green, orange, and purple, respectively. The shaded orange area corresponding to the times when the large BrO hotspot from 26 March to 4 April 2007 is predicted to be observed at the three Arctic sites and then transported to the sub-Arctic sites.

that are more depleted. Morin et al. (2005) report that dynamic conditions of the boundary layer near the shore can lead to very different surface O_3 behaviors observed at Alert compared to at a site over the sea ice 10 km away. Similar results were found by Jacobi et al. (2006) when comparing O_3 observations at Zeppelin Station and nearby ($\sim$ 100–200 km) ship-based measurements. The coarse resolution of our simulation ($2^\circ \times 2.5^\circ$) and the general difficulty of models in reproducing boundary layer depth and vertical mixing processes could thus be one explanation for our poor representa-

tion of ODEs at some of these surface sites. Another explanation is the lack of detailed chlorine chemistry in this version of GEOS-Chem. In particular, we do not consider acid displacement of Cl^- in SSA (Keene et al., 2007) which, together with bromine chemistry, could act to enhance ODEs. Finally, our simulation does not include local snowpack Br activation, which has been shown to lead to surface ODEs when the stable Arctic boundary layer is decoupled from convective exchange with the free troposphere (Custard et al., 2017; Peterson et al., 2015, 2017; Pratt et al., 2013; S. Wang et al., 2019).

4.2 Spatiotemporal distribution of O_3 depletion in GEOS-Chem

Figure 9 shows the spatial distribution of monthly mean surface O_3 mixing ratios calculated in the FYI+MYI Snow simulation as well as the decrease in surface O_3 (ΔO_3) relative to the STD simulation for March and April 2007–2009. The lowest monthly mean O_3 mixing ratios are ~ 25 ppbv in March over the Canadian Arctic Archipelago and ~ 20–25 ppbv in April over the North Pole (Fig. 9a), with a spatial distribution corresponding to that of the simulated VCD_{tropo} (Fig. 2). Note that the low O_3 values simulated over Europe are due to NO_x titration. The monthly mean values from the FYI+MYI Snow simulation are within 8 ppbv of surface observations at Utqiaġvik (model versus observation: March 28 ppbv versus 22 ppbv and April 28 ppbv versus 20 ppbv), Alert (model versus observation: March 29 ppbv versus 33 ppbv and April 27 ppbv versus 27 ppbv), Zeppelin (model versus observation: March 32 ppbv versus 39 ppbv and April 27 ppbv versus 31 ppbv), and Elk Island (model versus observation: March 28 ppbv versus 36 ppbv and April 35 ppbv versus 38 ppbv). The mean values of surface ΔO_3 increase from 4–8 ppbv (15 %–30 % depletion relative to the STD simulation) in March to 8–14 ppbv (30 %–40 %) in April, when sufficient sunlight is available to drive photochemistry at high latitudes (Fig. 9b). Poleward of 60° N, the FYI+MYI Snow simulation displays a pan-Arctic O_3 decrease of 3.7 ppbv (11 %) in March and 8.3 ppbv (23 %) relative to the STD simulation.

We define the frequency of ODEs as the percent of time when more than 20 ppbv O_3 is lost due to blowing snow ($\Delta O_3 > 20$ ppbv; Fig. 9c). Applying this definition to the FYI+MYI Snow simulation, we find that ODEs occur up to 1 %–5 % of the time in March, increasing to up to 15 %–25 % of the time in April as sunlight extends to higher latitudes (Fig. 9c). Using an ODE definition including more moderate events ($\Delta O_3 > 10$ ppbv), we find that poleward of 70° N ODEs occur 20 %–60 % of the time in April (Fig. 9d). The median aerial extent of ODEs ($\Delta O_3 > 20$ ppbv) simulated in the FYI+MYI Snow simulation is 0.35×10^6 km^2 (horizontal extent of ~ 330 km), with some of the largest ODEs extending over areas of $1.5–7 \times 10^6$ km^2 (~ 700–1500 km horizontal extent). Our results are consistent with the 282 km median size of major ODEs inferred by Halfacre et al. (2014) using ice-tethered buoys combined with back trajectories.

The decrease in surface O_3 due to blowing-snow SSA is 60 % larger in the FYI+MYI Snow simulation compared to the FYI Snow simulation (Fig. 10a). The time series of pan-Arctic daily mean ΔO_3 for the FYI+MYI Snow simulation at different altitudes shows that ΔO_3 is uniform in the bottom 500 m altitude and extends to 1000 m altitude, where the model-calculated ΔO_3 is about half of the surface ΔO_3. At 2000 m, ΔO_3 is generally below 4 ppbv (Fig. 10b). This is consistent with ozonesonde profiles, which indicate that depletion events are confined to the lowest 1000 m with an average height of the top of the layer at 500 m (Hopper et al., 1998; Oltmans et al., 2012; Tarasick and Bottenheim, 2002). We find that the Arctic tropospheric O_3 burden ($> 60°$ N) decreases by 3 % in March and 6 % in April in the FYI+MYI simulation relative to the STD simulation.

In our simulation, the timing of the maximum ΔO_3 takes place 4–5 d after the maximum in the blowing-snow SSA burden (Figs. 4c and 10b), reflecting increasing O_3 loss as BrO concentrations increase. This is illustrated during the 25–30 March 2007 event: the pan-Arctic blowing-snow SSA burden and VCD_{tropo} reach their maximum values on 27 March, while the lowest values for surface O_3 occur 4 d later on 31 March (Fig. 5, bottom row). By 29–30 March the blowing-snow SSA burden is back to low values over the Arctic, but the VCD_{tropo} values are still elevated, and low surface O_3 mixing ratios are predicted throughout the Arctic. This can be explained by the different lifetimes of these species over the springtime Arctic: ~ 1 d for SSA, 4–7 d for the Br_y family (consisting of all the gas-phase inorganic bromine species), and 30–40 d for O_3.

4.3 Transport of O_3-depleted Arctic air to lower latitudes

In some instances, large-scale blowing-snow-induced bromine activation can influence surface O_3 in sub-Arctic regions. The large BrO explosion and associated O_3 depletion from late March to early April 2007 (Fig. 4a and b) illustrate this. The light-orange shading in Fig. 8 corresponds to the times when this BrO explosion is transported to the three Arctic sites and several sub-Arctic sites. The GEOS-Chem FYI+MYI Snow simulation shows the transport of O_3-depleted air to Utqiaġvik on 25–27 March 2007, with observations showing much stronger depletion than the model (Fig. 8a). This air mass is observed at Alert on 31 March–4 April, and the eastern edge of that O_3-depleted air reaches Zeppelin around the same time (Fig. 8b, c). The O_3-depleted air is then transported southward over Hudson Bay and towards the northeastern United States on 4–9 April (Figs. 5 and 11), mostly below 1000 m altitude. At the synoptic level, a surface low was sweeping across the United States from the central Rockies to the Great Lakes in early April, bringing sub-freezing Arctic air behind its cold front

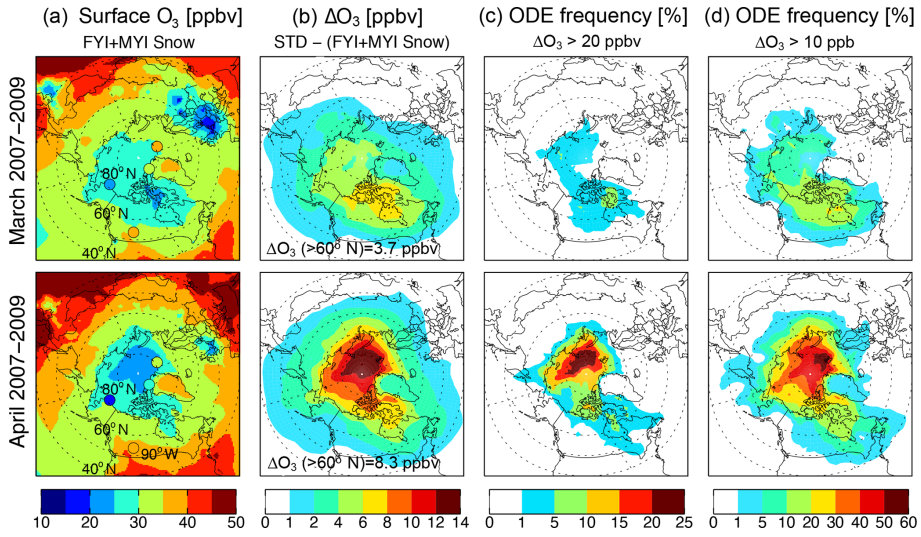

Figure 9. Monthly mean distribution of surface O_3 simulated with GEOS-Chem for March (top row) and April (bottom row) 2007–2009. **(a)** Surface O_3 mixing ratios in the GEOS-Chem FYI+MYI Snow simulation. The circles are color-coded by monthly mean surface O_3 observed at three Arctic (Utqiaġvik, Alert, and Zeppelin) and one sub-Arctic site (Elk Island). **(b)** Decrease in surface O_3 (ΔO_3, ppbv) due to blowing snow obtained as the difference between the STD and FYI+MYI Snow simulations. **(c)** Occurrence frequency of ODEs (in %), defined as the percent of time that more than 20 ppbv of O_3 is lost due to blowing snow ($\Delta O_3 > 20$ ppbv). **(d)** Occurrence frequency of ODEs, defined as $\Delta O_3 > 10$ ppbv.

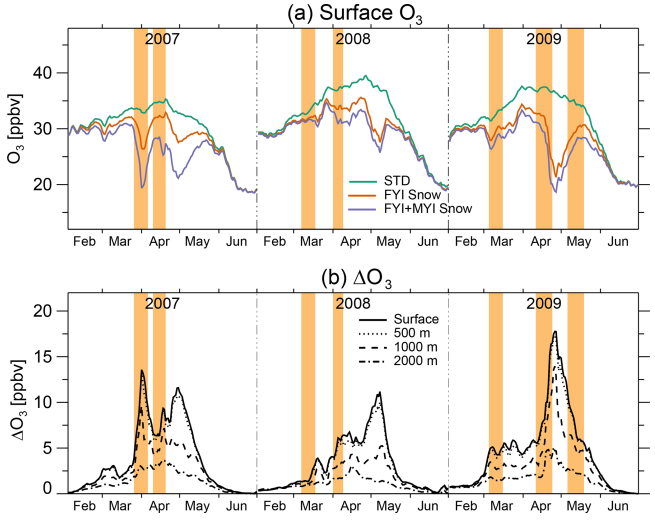

Figure 10. Time series of daily mean surface O_3 and decrease in surface O_3 (ΔO_3) due to blowing snow at high latitudes ($> 60°$ N) between February and June 2007–2009. **(a)** Daily mean surface O_3 mixing ratios averaged poleward of 60° N for the STD (blue line), FYI Snow (purple), and FYI+MYI Snow (red line) GEOS-Chem simulations. **(b)** Daily mean ΔO_3, obtained as the difference between the FYI+MYI Snow and STD simulations at the surface (solid line), 500 m altitude (dotted line), 1000 m altitude (dashed line), and 2000 m altitude (dash-dotted line). The events highlighted in light orange are defined as periods when GOME-2 or OMI BrO hotspots cover more than 2×10^6 km^2 for longer than 5 d.

with record-breaking cold temperatures being measured over the central plains and much of the southeastern United States (NOAA/USDA, 2008).

Between 2 and 7 April, observed O_3 mixing ratios at five sub-Arctic sites from Elk Island (53.7° N) to Woodstock (43.9° N) decreased from background levels of 40 ppbv down to 10–20 ppbv (Fig. 8). This decrease is reproduced by both the FYI and FYI+MYI Snow simulations, which show that enhanced VCD_{tropo} and blowing-snow SSA were transported over Hudson Bay towards the Great Lakes region (Fig. 11a–c). By the time the polar air mass reached the northeastern United States, the BrO VCD_{tropo} were back to normal levels, but because of its longer lifetime, O_3 was 5–10 ppbv lower than background mixing ratios as shown by the FYI+MYI Snow simulation (Fig. 11d). This decrease in surface O_3 was observed at NAPS and CASTNET surface sites throughout southeastern Canada and the northeastern United States (Fig. 11d).

Ridley et al. (2007) discuss a similar transport event of O_3-depleted air from the Canadian Arctic Archipelago and nearby Arctic Ocean to Hudson Bay observed in April 2000 during the Tropospheric Ozone Production about the Spring Equinox (TOPSE) aircraft campaign. During that event, O_3 levels were reduced from 30 to 40 ppbv down to values as low as 0.5 ppbv in a large area below 500 m altitude. Over the 3-year period that we examined, our simulations suggest that transport of O_3-depleted air ($\Delta O_3 > 20$ ppbv) to Hudson Bay occurs 1 %–10 % of the time (0.3–3 d per month) in March and in April (Fig. 9c), with the transport of more moderate O_3 depletion ($\Delta O_3 > 10$ ppbv) taking place 10 %–20 %

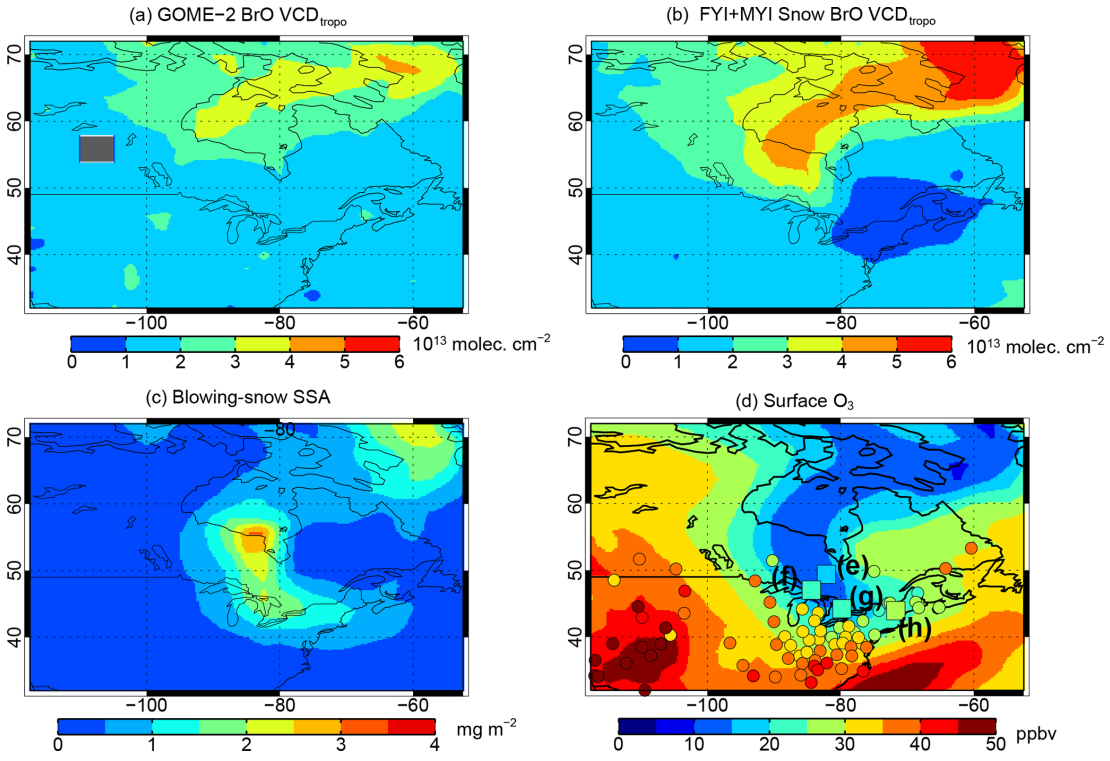

Figure 11. Mean 5–9 April 2007 VCD_{tropo} for **(a)** GOME-2 and **(b)** the GEOS-Chem FYI+MYI Snow simulation. Mean 5–9 April 2007 **(c)** blowing-snow SSA burden and **(d)** surface O_3 mixing ratios for 5–9 April 2007 from the GEOS-Chem FYI+MYI Snow simulation. Surface O_3 observations are shown as color-coded symbols in panel **(d)**, with the squares corresponding to the sub-Arctic sites from Fig. 8. The letter numbering for **(e)**–**(h)** corresponds to the panel numbers in Fig. 8.

of the time (3–6 d per month). In March–April 2008, measurements in the ice-free North Atlantic showed the transport of O_3-poor air from the Arctic basin down to 52° N during the ICEALOT cruise (Gilman et al., 2010): a 13 ppbv decrease in O_3 was accompanied by a simultaneous decrease in the acetylene-to-benzene ratio, indicating exposure to halogen oxidation. In our simulation, we find that the transport of air mass with $\Delta O_3 > 10$ ppbv air to sub-Arctic latitudes occurs with a frequency of 5 %–10 % (1.5–3 d per month) down to 50° N and 1 %–5 % (< 1.5 d per month) down to 40° N (Fig. 9d) and that this transport appears to be favored over Hudson Bay extending to the northeastern United States and the western Atlantic off Nova Scotia (Fig. 9d). At mid-latitudes (30–60° N), the FYI+MYI Snow simulation results in a mean surface O_3 decrease of 1.2 ppbv (3.3 %) in March–April, thus a small but non-negligible contribution.

5 Atmospheric deposition on snow as a source of salinity and bromide

We use the results of the FYI Snow simulation to examine the potential role of the atmospheric deposition of SSA and gas-phase Br_y as a source of salinity and bromide to snow on sea ice. Snow composition profiles indicate that atmospheric deposition can sometimes be a more important source of salinity and Br^- than upward brine migration, especially over MYI and in deep snowpack (> 10–17 cm) over FYI (Domine et al., 2004; Krnavek et al., 2012; Peterson et al., 2019). Figure 12a shows the evolution of deposition on sea ice (poleward of 60° N) for Na^+ and for total bromine (sum of particulate Br^- and gas-phase Br_y) in the GEOS-Chem FYI Snow simulation. Between September and May, the deposition of Na^+ on snow-covered sea ice has an average daily value of 2.2×10^6 kg d^{-1}. For total bromine (SSA Br^- and gas-phase Br_y), the average daily value is 6.7×10^4 kg d^{-1}. Open-ocean SSA and blowing-snow SSA account nearly equally to these deposition fluxes.

From October to March the deposition of total bromine tracks that of Na^+, as both are derived from SSA (Fig. 12a). Starting in late March, the deposition of Na^+ decreases rapidly following the decrease in blowing-snow SSA emissions (Fig. 4c) due to slower wind speeds and warmer temperatures (Huang and Jaeglé, 2017). The deposition of bromine remains high for another month, however, as once bromine activation starts in early spring, a large fraction of Br deposition is in the form of Br_y, in particular HBr, which is the end product of reactive bromine chemistry. In April–May, deposition of Br_y accounts for more than half of total bromine deposition (Fig. 12a). As Br_y has a longer life-

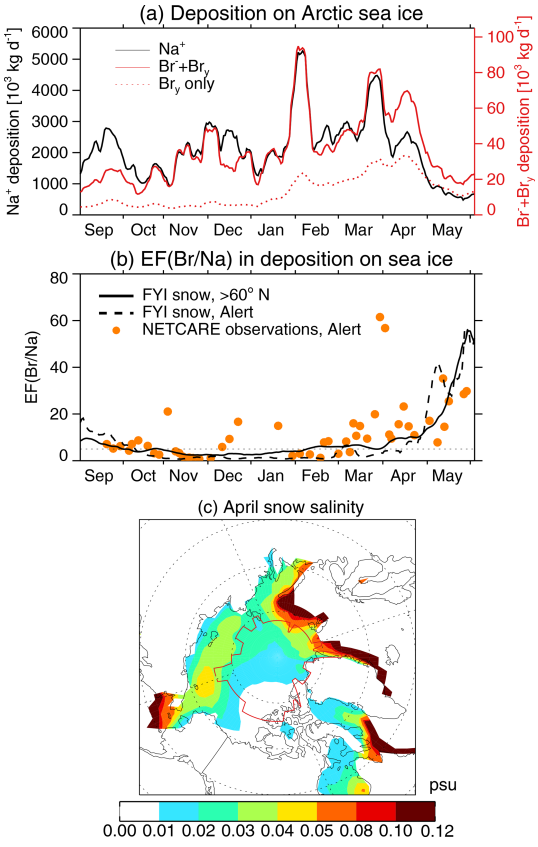

Figure 12. Modeled evolution of the deposition and Br/Na enrichment factor on sea ice (> 60° N) for 2007 calculated with the FYI Snow simulation. **(a)** Total deposition on sea ice (in units of 10^3 kg d^{-1}) for Na^+ (black line, left axis), $Br^- + Br_y$ (red line, right axis), and Br_y only (dashed red line, right axis). **(b)** Modeled Br/Na enrichment factor (EF; black line) relative to seawater in deposition over sea ice; see Sect. 5 for the definition of EF. The orange circles show the enrichment factors observed during the NETCARE campaign at Alert, Nunavut (Macdonald et al., 2017). The dashed black line is the modeled EF sampled at Alert. A 10 d boxcar smoothing has been applied to all the modeled time series between September and May. The horizontal dotted line represents the value EF=5, assumed for the emitted blowing-snow SSA. **(c)** Surface snow salinity due to the cumulative SSA deposition on sea ice for 1 February–30 April assuming a 1 cm snow accumulation rate for that period (see text). The red line shows the location of MYI.

time against deposition than particulate Br^- and Na^+, Br_y shows a more gradual decrease in deposition in April and May. This behavior is consistent with observations of freshly fallen snow at Alert during the Network on Climate and Aerosols Research (NETCARE) campaign, showing a broad spring peak in Br^- deposition between late March and late May (Macdonald et al., 2017). A similar increase of Br^- in snowfall samples after polar sunrise was reported at Alert by Toom-Sauntry and Barrie (2002). Furthermore, Spolaor et al. (2013, 2014) found a strong seasonal variability of Br^- in polar firn at both Arctic and Antarctic sites, with greater Br^- values in spring and summer compared to winter.

We derive the Br^- / Na^+ enrichment factor (EF) of deposition relative to seawater composition (which has a Br^-/Na^+ mass ratio of 0.00625 g g^{-1}) as

$$\mathrm{EF} = \left(\frac{[\mathrm{Br}^- + \mathrm{Br}_y]}{[\mathrm{Na}^+]}\right)_{\text{deposition}} / \left(\frac{[\mathrm{Br}^-]}{[\mathrm{Na}^+]}\right)_{\text{seawater}}. \quad (1)$$

EF is calculated for each day and each model grid box and then surface-area-weighted over sea ice to obtain the daily time series of pan-Arctic EF shown in Fig. 12b. The model-calculated EF is fairly constant between September and February, with values of ∼ 3–10. Starting in late March, the divergence between bromine and Na^+ deposition leads to an increase in EF to a value of 14 by the end of April, followed by a more rapid increase in May up to a value of ∼ 60. In May, the mean model-calculated EF of deposition is 30. These values are remarkably consistent with the EF measured during the NETCARE campaign at Alert (Macdonald et al., 2017), as shown in Fig. 12b, with mean observed values of EF ∼ 7 between September and February, 15 in April, and 25 in May. Similarly, Toom-Sauntry and Barrie (2002) observed an increase in EF from low enrichment in the dark winter months (median of 1.5–5) to a large enrichment (median of 20–72) after polar sunrise. In our simulation of the blowing-snow SSA, we assumed a constant value of EF = 5, which appears to underestimate the EF of snow in May by a factor of 2–3. This springtime increase in the enrichment of Br^- in snow over sea ice could thus act to propagate bromine explosions and ODEs into May and could explain our systematic underestimation of observed VCD_{tropo} in May. Using a one-dimensional model, Piot and von Glasow (2008) compared modeled and observed deposition on snow at Utqiaġvik, demonstrating that 75 % of deposited bromine may be re-emitted into the gas phase as Br_2 or BrCl. They proposed that cycles of deposition and re-emissions of bromine from snow could thus result in a "leap-frogging" process and explain the observations of the progressive Br^- enrichment of snow in coastal Arctic regions with distance inland (Simpson et al., 2005). Indeed, Peterson et al. (2018) observed enhanced BrO up to 200 km inland over snow-covered tundra near Utqiaġvik. Our simulations suggest that a similar mechanism could occur in snow over sea ice via repeated cycles of blowing-snow SSA sublimation and the deposition of reactive bromine. These cycles could thus be important in propagating bromine explosions in space (onto coastal snow-covered land) as well as in time on sea ice (into late spring).

We now use the model-simulated Na^+ deposition (FYI Snow simulations) on the sea-ice-covered Arctic Ocean to estimate the salinity of surface snow due to SSA deposition. In our simulation, wet and dry deposition contribute nearly equally to SSA deposition. Over the 3-month period between 1 February and 31 April, the cumulative SSA deposition on

Arctic sea ice is 10.3×10^8 kg SSA in the FYI Snow simulation. Snow depth on sea ice is not calculated in MERRA-2, and reanalyses tend to have highly uncertain solid precipitation in polar regions (Lindsay et al., 2014; Uotila et al., 2019), so we rely on the limited observations available. The Warren et al. (1999) climatology, which is based on 1954–1991 Soviet drifting stations measurements on Arctic MYI, shows that snow depth increases from 29.7 to 34.4 cm during these 3 months, resulting in 4.7 cm snow accumulation. This is likely an overestimate of the pan-Arctic snow depth because MYI tends to have thicker snow and these measurements represent conditions from past decades (Kwok and Cunningham, 2008). Indeed, the 2003–2008 AMSR-E (Advanced Microwave Scanning Radiometer for the Earth Observing System) snow depth retrievals over FYI compiled by Zygmuntowska et al. (2014) show much lower snow depths, increasing from 18 cm in February to 19 cm in May, thus a 1 cm snow accumulation. These two estimates in snow accumulation result in pan-Arctic snow accumulations of 10^{14} to 2.2×10^{13} kg (sea ice extent is 11×10^6 km^2, and fresh snow has a density of 200 kg m^{-3}), which combined with our calculated SSA deposition results in a mean salinity of 0.01–0.04 psu of surface snow due to deposition. Figure 12c shows the spatial distribution of snow salinity due to SSA deposition assuming a 1 cm snow accumulation. High salinities (> 0.05 psu) are calculated in sea ice regions near the ice-free open ocean in the North Atlantic and Bering Sea, with lower values on FYI (0.02–0.05 psu) and MYI (0.01–0.03 psu). Deposition could thus represent a significant source of salinity of surface snow on MYI by the time sunrise reaches high latitudes, and it could also be important for FYI as the snow gets deeper in late spring (Petty et al., 2018; Warren et al., 1999).

6 Conclusions

We used the GEOS-Chem model to examine the impact of blowing-snow SSA on bromine chemistry and O_3 during Arctic spring. We conducted two blowing-snow simulations assuming a 0.1 psu surface snow salinity on FYI and different salinities on MYI (0.01 psu for the FYI Snow simulation and 0.05 psu for the FYI+MYI Snow simulation). We evaluated these simulations against satellite observations of VCD_{tropo} from GOME-2 and OMI for 2007–2009. We found that our simulations reproduce the spatiotemporal distribution of the observed VCD_{tropo} to within -12 % to $+17$ % in March and April and capture the spatial extent as well as the frequency of most large BrO hotspots in March and April. However, our simulations predicted too rapid a decrease in VCD_{tropo} in May, while observations showed a more gradual decrease. The FYI+MYI Snow simulation captured observed BrO hotspots over the North Pole better than the FYI Snow simulation. In our FYI+MYI simulation, blowing-snow SSA emissions on MYI account for 20 %–30 % of the VCD_{tropo} enhancement and thus represent a significant source of bromine activation. In the past, the search for halogen-containing substrates in polar regions has often focused on the role of frost flowers, newly formed sea ice, and FYI snowpack on polar halogen activation because of the higher salinity of these surfaces and of their snowpack relative to MYI (e.g., Abbatt et al., 2012; Jacobi et al., 2006; Kaleschke et al., 2004; Simpson et al., 2007a; Yang et al., 2010). Our simulations suggest that the role of MYI in halogen activation is likely also important, consistent with results of several studies (Choi et al., 2018; Gilman et al., 2010; Halfacre et al., 2014; Peterson et al., 2019).

The inclusion of blowing-snow SSA in our FYI+MYI Snow simulation results in a pan-Arctic decrease in surface O_3 of 3.7 ppbv (11 %) in March and 8.3 ppbv (23 %) in April. As most of this decrease is confined to altitudes below 1000 m, the Arctic tropospheric O_3 burden decreases by only 3 %–6 % in March–April. Compared to surface O_3 observations at coastal Arctic sites, we find that our simulation captures only 25 %–40 % of observed ODEs and often underestimates their magnitude. The FYI+MYI simulation misses 60 %–75 % of observed ODEs, in particular the early March events at Utqiaġvik and most of the May events at Utqiaġvik, Alert, and Zeppelin. The simulation does reproduce an event of low O_3 Arctic air transport down to 40° N, which was observed at multiple sub-Arctic surface sites. We estimate that these transport events occur in March and April with a frequency of 1.5–3 d per month down to 50° N and < 1.5 d per month down to 40° N.

The mixed success of our simulation at capturing the rapid O_3 variations observed at coastal Arctic sites could be related to the coarse resolution of the model, the difficulty in simulating Arctic boundary layer exchange processes, the lack of detailed chlorine chemistry, or the fact that we did not include direct halogen activation by snowpack chemistry. The locations of the three coastal Arctic sites with surface O_3 observations correspond to GEOS-Chem grid box sizes of $\sim$ 40–90 km (latitude) by 220 km (longitude). It is thus not surprising that we are not able to capture some surface O_3 events which have been shown to have large variability on scales of 10–100 km (Morin et al., 2005; Jacobi et al., 2006). Most reanalyses, including MERRA-2, tend to simulate Arctic surface temperature inversions that are too weak, likely due to their low skill simulating turbulent heat fluxes over sea ice (Graham et al., 2019). Excessive exchange between the boundary layer and free troposphere would transport O_3-rich free-tropospheric air down to the surface, which might explain our simulations of ODEs that are too weak compared to observations. The influence of snowpack bromine chemistry was examined in two previous modeling studies (Falk and Sinnhuber, 2018; Toyota et al., 2011). These studies displayed remarkable agreement with surface O_3 observations, in particular at Alert and Utqiaġvik, and reproduced the synoptic variability in GOME VCD values. However, both studies systematically underestimated the magnitude of ob-

served BrO VCDs by at least a factor of 2. These results together with our GEOS-Chem blowing-snow simulations suggest that most of the VCD_{tropo} enhancements observed by satellites can be explained by blowing-snow SSA leading to BrO enhancements over larger vertical (0–2 km) and horizontal scales (pan-Arctic) than snowpack chemistry, but that in the shallow boundary layer ($\sim$ 50–250 m) over the springtime Arctic direct snowpack halogen activation could contribute to Br release and potentially be responsible for the most severe ODEs. Indeed, some of the strongest ODEs observed at the surface seem to occur when the stable Arctic boundary layer is decoupled from convective exchange with the free troposphere (Moore et al., 2014; Seabrook et al., 2011; S. Wang et al., 2019). Furthermore, as boundary layer O_3 reaches very low levels (< 4 ppbv), BrO production via Reaction (R3) is suppressed, and atomic Br becomes much more abundant than BrO (Neuman et al., 2010; S. Wang et al., 2019), such that satellites would not necessarily observe co-located O_3 depletion and enhanced BrO VCD_{tropo}.

Based on our analysis of the seasonal variation in the modeled deposition of Na^+ and bromine on snow, we propose that the progressive enrichment of bromine in deposition onto sea ice could help propagate blowing-snow SSA bromine activation into May, even as the magnitude of blowing-snow SSA emissions starts to decrease. The increase of our calculated springtime enrichment of Arctic snow Br^- is similar to observations showing a peak after polar sunrise (Macdonald et al., 2017; Spolaor et al., 2013; Toom-Sauntry and Barrie, 2002). The recycling of deposited bromine was previously proposed in the context of frost flower or snowpack activation followed by inland transport over coastal regions (Domine et al., 2004; Piot and von Glasow, 2008; Simpson et al., 2005, 2007b). We propose that a similar mechanism takes place over sea ice and snow-covered coastal regions with blowing-snow SSA, enabling BrO explosions to propagate spatially and to last longer into late spring. We also show that SSA deposition to surface snow in winter and spring, when snow accumulation on sea ice is at its minimum, could account for 0.01–0.03 psu on MYI, 0.02–0.05 psu on FYI, and > 0.1 psu on sea ice areas close to the open ocean. While upward migration of brine from sea ice is the main source of salinity in surface snow over FYI with shallow snowpack, atmospheric deposition could thus be the dominant source in surface snow over the less saline MYI sea ice and could play an important role in late spring as the snowpack deepens over FYI (Domine et al., 2004; Krnavek et al., 2012; Peterson et al., 2019).

Our simulations did not include two-way coupling between snowpack composition and atmospheric deposition, did not consider blowing snow on coastal snow enriched in Br^-, and did not incorporate direct snowpack halogen activation. Incorporating these coupled processes together with blowing-snow SSA promises to yield further insights into the mechanisms leading to polar bromine activation and ODEs. In addition, further examination of how horizontal resolution and turbulent mixing parameterizations influence simulations of ODEs would help improve our understanding of the interplay between meteorology and chemistry in inducing rapid variations in surface O_3 over the Arctic.

Data availability. The GOME-2 VCD_{tropo} data are available upon request from Nicolas Theys (nicolas.theys@aeronomie.be). The OMI VCD_{tropo} data are available upon request from Sungyeon Choi (sungyeon.choi@nasa.gov). The surface O_3 observations from surface monitoring sites are available from the EBAS database (http://ebas.nilu.no; EBAS, 2019), CAPMoN (http://donnees.ec.gc.ca/data/air/monitor/monitoring-of-atmospheric-gases/ground-level-ozone/; CAPMoN, 2019), NAPS (https://www.canada.ca/en/environment-climate-change/services/air-pollution/monitoring-networks-data.html; Environment Canada, 2019), and CASTNET (https://www.epa.gov/castnet/castnet-ozone-monitoring; EPA, 2019) data repositories. The GEOS-Chem simulations are available upon request from the corresponding author (jaegle@uw.edu).

Supplement. The supplement related to this article is available online at: https://doi.org/10.5194/acp-20-7335-2020-supplement.

Author contributions. JH and LJ designed the study, conducted the GEOS-Chem simulations, and analyzed the results. QC, BA, TS, and MJE contributed to model development. NT and SC provided the tropospheric BrO columns for GOME-2 and OMI. JH wrote the paper with significant contributions from LJ. All the authors contributed to editing the paper.

Competing interests. The authors declare that they have no conflict of interest.

Financial support. This research has been supported by NASA (grant nos. NNX15AE32G and 80NSSC19K1273).

Review statement. This paper was edited by Jayanarayanan Kuttippurath and reviewed by two anonymous referees.

References

Abbatt, J. P. D., Thomas, J. L., Abrahamsson, K., Boxe, C., Granfors, A., Jones, A. E., King, M. D., Saiz-Lopez, A., Shepson, P. B., Sodeau, J., Toohey, D. W., Toubin, C., von Glasow, R., Wren, S. N., and Yang, X.: Halogen activation via interactions with environmental ice and snow in the polar lower troposphere and other regions, Atmos. Chem. Phys., 12, 6237–6271, https://doi.org/10.5194/acp-12-6237-2012, 2012.

Alvarez-Aviles, L., Simpson, W. R., Douglas, T. A., Sturm, M., Perovich, D., and Domine, F.: Frost flower chemical composition during growth and its implications for aerosol production and bromine activation, J. Geophys. Res.-Atmos., 113, D21304, https://doi.org/10.1029/2008JD010277, 2008.

AMAP: AMAP Assessment 2011: Mercury in the Arctic, Arctic Monitoring and Assessment Programme (AMAP), Oslo, Norway, 193 pp., available at: https://www.amap.no/documents/doc/amap-assessment-2011-mercury-in-the-arctic/90 (last access: 13 July 2018), 2011.

Ammann, M., Cox, R. A., Crowley, J. N., Jenkin, M. E., Mellouki, A., Rossi, M. J., Troe, J., and Wallington, T. J.: Evaluated kinetic and photochemical data for atmospheric chemistry: Volume VI – heterogeneous reactions with liquid substrates, Atmos. Chem. Phys., 13, 8045–8228, https://doi.org/10.5194/acp-13-8045-2013, 2013.

Barrie, L. A., Bottenheim, J. W., Schnell, R. C., Crutzen, P. J., and Rasmussen, R. A.: Ozone destruction and photochemical reactions at polar sunrise in the lower Arctic atmosphere, Nature, 334, 138–141, https://doi.org/10.1038/334138a0, 1988.

Begoin, M., Richter, A., Weber, M., Kaleschke, L., Tian-Kunze, X., Stohl, A., Theys, N., and Burrows, J. P.: Satellite observations of long range transport of a large BrO plume in the Arctic, Atmos. Chem. Phys., 10, 6515–6526, https://doi.org/10.5194/acp-10-6515-2010, 2010.

Bey, I., Jacob, D. J., Yantosca, R. M., Logan, J. A., Field, B. D., Fiore, A. M., Li, Q. B., Liu, H. G. Y., Mickley, L. J., and Schultz, M. G.: Global modeling of tropospheric chemistry with assimilated meteorology: Model description and evaluation, J. Geophys. Res.-Atmos., 106, 23073–23095, https://doi.org/10.1029/2001JD000807, 2001.

Blechschmidt, A.-M., Richter, A., Burrows, J. P., Kaleschke, L., Strong, K., Theys, N., Weber, M., Zhao, X., and Zien, A.: An exemplary case of a bromine explosion event linked to cyclone development in the Arctic, Atmos. Chem. Phys., 16, 1773–1788, https://doi.org/10.5194/acp-16-1773-2016, 2016.

Bottenheim, J. W. and Chan, E.: A trajectory study into the origin of spring time Arctic boundary layer ozone depletion, J. Geophys. Res.-Atmos., 111, D19301, https://doi.org/10.1029/2006JD007055, 2006.

Bottenheim, J. W., Gallant, A. G., and Brice, K. A.: Measurements of NOY species and O_3 at 82° N latitude, Geophys. Res. Lett., 13, 113–116, https://doi.org/10.1029/GL013i002p00113, 1986.

Bottenheim, J. W., Netcheva, S., Morin, S., and Nghiem, S. V.: Ozone in the boundary layer air over the Arctic Ocean: measurements during the TARA transpolar drift 2006–2008, Atmos. Chem. Phys., 9, 4545–4557, https://doi.org/10.5194/acp-9-4545-2009, 2009.

CAPMoN: Ground-Level Ozone, available at: http://donnees.ec.gc.ca/data/air/monitor/monitoring-of-atmospheric-gases/ground-level-ozone/, last access: 1 November 2019.

Chen, Q., Schmidt, J. A., Shah, V., Jaeglé, L., Sherwen, T., and Alexander, B.: Sulfate production by reactive bromine: Implications for the global sulfur and reactive bromine budgets, Geophys. Res. Lett., 44, 7069–7078, https://doi.org/10.1002/2017GL073812, 2017.

Choi, S., Wang, Y., Salawitch, R. J., Canty, T., Joiner, J., Zeng, T., Kurosu, T. P., Chance, K., Richter, A., Huey, L. G., Liao, J., Neuman, J. A., Nowak, J. B., Dibb, J. E., Weinheimer, A. J., Diskin, G., Ryerson, T. B., da Silva, A., Curry, J., Kinnison, D., Tilmes, S., and Levelt, P. F.: Analysis of satellite-derived Arctic tropospheric BrO columns in conjunction with aircraft measurements during ARCTAS and ARCPAC, Atmos. Chem. Phys., 12, 1255–1285, https://doi.org/10.5194/acp-12-1255-2012, 2012.

Choi, S., Theys, N., Salawitch, R. J., Wales, P. A., Joiner, J., Canty, T. P., Chance, K., Suleiman, R., Palm, S. P., Cullather, R. I., Darmenov, A. S., da Silva, A., Kurosu, T. P., Hendrick, F., and Van Roozendael, M.: Link between Arctic tropospheric BrO explosion observed from space and sea salt aerosols from blowing snow investigated using Ozone Monitoring Instrument (OMI) BrO data and GEOS-5 data assimilation system, J. Geophys. Res.-Atmos., 123, 6954–6983, https://doi.org/10.1029/2017JD026889, 2018.

Custard, K. D., Raso, A. R. W., Shepson, P. B., Staebler, R. M., and Pratt, K. A.: Production and Release of Molecular Bromine and Chlorine from the Arctic Coastal Snowpack, Acs Earth Space Chem., 1, 142–151, https://doi.org/10.1021/acsearthspacechem.7b00014, 2017.

Domine, F., Sparapani, R., Ianniello, A., and Beine, H. J.: The origin of sea salt in snow on Arctic sea ice and in coastal regions, Atmos. Chem. Phys., 4, 2259–2271, https://doi.org/10.5194/acp-4-2259-2004, 2004.

Donlon, C. J., Martin, M., Stark, J., Roberts-Jones, J., Fiedler, E., and Wimmer, W.: The Operational Sea Surface Temperature and Sea Ice Analysis (OSTIA) system, Remote Sens. Environ., 116, 140–158, https://doi.org/10.1016/j.rse.2010.10.017, 2012.

EBAS: EMEP dataBASe, Norwegian Institute for Air Research, available at: http://ebas.nilu.no, last access: 1 November 2019.

Ebinghaus, R., Kock, H. H., Temme, C., Einax, J. W., Lowe, A. G., Richter, A., Burrows, J. P., and Schroeder, W. H.: Antarctic springtime depletion of atmospheric mercury, Environ. Sci. Technol., 36, 1238–1244, https://doi.org/10.1021/es015710z, 2002.

Environment Canada: NAPS: National Air Pollution Surveillance Program, available at: https://www.canada.ca/en/environment-climate-change/services/air-pollution/monitoring-networks-data.html, last access: 1 November 2019.

EPA: Clean Air Status and Trends Network (CASTNET), available at: https://www.epa.gov/castnet/castnet-ozone-monitoring, last access: 1 November 2019.

Falk, S. and Sinnhuber, B.-M.: Polar boundary layer bromine explosion and ozone depletion events in the chemistry–climate model EMAC v2.52: implementation and evaluation of AirSnow algorithm, Geosci. Model Dev., 11, 1115–1131, https://doi.org/10.5194/gmd-11-1115-2018, 2018.

Fan, S.-M. and Jacob, D. J.: Surface ozone depletion in Arctic spring sustained by bromine reactions on aerosols, Nature, 359, 522–524, https://doi.org/10.1038/359522a0, 1992.

Fischer, E. V., Jacob, D. J., Yantosca, R. M., Sulprizio, M. P., Millet, D. B., Mao, J., Paulot, F., Singh, H. B., Roiger, A., Ries, L., Talbot, R. W., Dzepina, K., and Pandey Deolal, S.: Atmospheric peroxyacetyl nitrate (PAN): a global budget and source attribution, Atmos. Chem. Phys., 14, 2679–2698, https://doi.org/10.5194/acp-14-2679-2014, 2014.

Fisher, J. A., Jacob, D. J., Travis, K. R., Kim, P. S., Marais, E. A., Chan Miller, C., Yu, K., Zhu, L., Yantosca, R. M., Sulprizio, M. P., Mao, J., Wennberg, P. O., Crounse, J. D., Teng, A. P., Nguyen, T. B., St. Clair, J. M., Cohen, R. C., Romer, P., Nault, B. A., Wooldridge, P. J., Jimenez, J. L., Campuzano-Jost, P., Day, D. A., Hu, W., Shepson, P. B., Xiong, F., Blake, D. R., Goldstein, A. H., Misztal, P. K., Hanisco, T. F., Wolfe, G. M., Ryerson, T. B., Wisthaler, A., and Mikoviny, T.: Organic nitrate chemistry and its implications for nitrogen budgets in an isoprene- and monoterpene-rich atmosphere: constraints from aircraft ($SEAC^4RS$) and ground-based (SOAS) observations in the Southeast US, Atmos. Chem. Phys., 16, 5969–5991, https://doi.org/10.5194/acp-16-5969-2016, 2016.

Frey, M. M., Norris, S. J., Brooks, I. M., Anderson, P. S., Nishimura, K., Yang, X., Jones, A. E., Nerentorp Mastromonaco, M. G., Jones, D. H., and Wolff, E. W.: First direct observation of sea salt aerosol production from blowing snow above sea ice, Atmos. Chem. Phys., 20, 2549–2578, https://doi.org/10.5194/acp-20-2549-2020, 2020.

Frieß, U., Hollwedel, J., Konig-Langlo, G., Wagner, T., and Platt, U.: Dynamics and chemistry of tropospheric bromine explosion events in the Antarctic coastal region, J. Geophys. Res.-Atmos., 109, D06305, https://doi.org/10.1029/2003JD004133, 2004.

Gelaro, R., McCarty, W., Suarez, M. J., Todling, R., Molod, A., Takacs, L., Randles, C. A., Darmenov, A., Bosilovich, M. G., Reichle, R., Wargan, K., Coy, L., Cullather, R., Draper, C., Akella, S., Buchard, V., Conaty, A., da Silva, A. M., Gu, W., Kim, G.-K., Koster, R., Lucchesi, R., Merkova, D., Nielsen, J. E., Partyka, G., Pawson, S., Putman, W., Rienecker, M., Schubert, S. D., Sienkiewicz, M., and Zhao, B.: The Modern-Era Retrospective Analysis for Research and Applications, Version 2 (MERRA-2), J. Climate, 30, 5419–5454, https://doi.org/10.1175/JCLI-D-16-0758.1, 2017.

Gilman, J. B., Burkhart, J. F., Lerner, B. M., Williams, E. J., Kuster, W. C., Goldan, P. D., Murphy, P. C., Warneke, C., Fowler, C., Montzka, S. A., Miller, B. R., Miller, L., Oltmans, S. J., Ryerson, T. B., Cooper, O. R., Stohl, A., and de Gouw, J. A.: Ozone variability and halogen oxidation within the Arctic and sub-Arctic springtime boundary layer, Atmos. Chem. Phys., 10, 10223–10236, https://doi.org/10.5194/acp-10-10223-2010, 2010.

Giordano, M. R., Kalnajs, L. E., Goetz, J. D., Avery, A. M., Katz, E., May, N. W., Leemon, A., Mattson, C., Pratt, K. A., and DeCarlo, P. F.: The importance of blowing snow to halogen-containing aerosol in coastal Antarctica: influence of source region versus wind speed, Atmos. Chem. Phys., 18, 16689–16711, https://doi.org/10.5194/acp-18-16689-2018, 2018.

Gong, S. L., Walmsley, J. L., Barrie, L. A., and Hopper, J. F.: Mechanisms for surface ozone depletion and recovery during polar sunrise, Atmos. Environ., 31, 969–981, https://doi.org/10.1016/S1352-2310(96)00264-6, 1997.

Graham, R. M., Cohen, L., Ritzhaupt, N., Segger, B., Graversen, R. G., Rinke, A., Walden, V. P., Granskog, M. A., and Hudson, S. R.: Evaluation of Six Atmospheric Reanalyses over Arctic Sea Ice from Winter to Early Summer, J. Climate, 32, 4121–4143, https://doi.org/10.1175/JCLI-D-18-0643.1, 2019.

Guenther, A. B., Jiang, X., Heald, C. L., Sakulyanontvittaya, T., Duhl, T., Emmons, L. K., and Wang, X.: The Model of Emissions of Gases and Aerosols from Nature version 2.1 (MEGAN2.1): an extended and updated framework for modeling biogenic emissions, Geosci. Model Dev., 5, 1471–1492, https://doi.org/10.5194/gmd-5-1471-2012, 2012.

Halfacre, J. W., Knepp, T. N., Shepson, P. B., Thompson, C. R., Pratt, K. A., Li, B., Peterson, P. K., Walsh, S. J., Simpson, W. R., Matrai, P. A., Bottenheim, J. W., Netcheva, S., Perovich, D. K., and Richter, A.: Temporal and spatial characteristics of ozone depletion events from measurements in the Arctic, Atmos. Chem. Phys., 14, 4875–4894, https://doi.org/10.5194/acp-14-4875-2014, 2014.

Hausmann, M. and Platt, U.: Spectroscopic measurement of bromine oxide and ozone in the high Arctic during Polar Sunrise Experiment 1992, J. Geophys. Res.-Atmos., 99, 25399–25413, https://doi.org/10.1029/94JD01314, 1994.

Hönninger, G. and Platt, U.: Observations of BrO and its vertical distribution during surface ozone depletion at Alert, Atmos. Environ., 36, 2481–2489, https://doi.org/10.1016/S1352-2310(02)00104-8, 2002.

Hopper, J. F., Barrie, L. A., Silis, A., Hart, W., Gallant, A. J., and Dryfhout, H.: Ozone and meteorology during the 1994 Polar Sunrise Experiment, J. Geophys. Res.-Atmos., 103, 1481–1492, https://doi.org/10.1029/97JD02888, 1998.

Huang, J. and Jaeglé, L.: Wintertime enhancements of sea salt aerosol in polar regions consistent with a sea ice source from blowing snow, Atmos. Chem. Phys., 17, 3699–3712, https://doi.org/10.5194/acp-17-3699-2017, 2017.

Huang, J., Jaeglé, L., and Shah, V.: Using CALIOP to constrain blowing snow emissions of sea salt aerosols over Arctic and Antarctic sea ice, Atmos. Chem. Phys., 18, 16253–16269, https://doi.org/10.5194/acp-18-16253-2018, 2018.

Jacobi, H.-W., Kaleschke, L., Richter, A., Rozanov, A., and Burrows, J. P.: Observation of a fast ozone loss in the marginal ice zone of the Arctic Ocean, J. Geophys. Res.-Atmos., 111, D15309, https://doi.org/10.1029/2005JD006715, 2006.

Jacobi, H.-W., Morin, S., and Bottenheim, J. W.: Observation of widespread depletion of ozone in the springtime boundary layer of the central Arctic linked to mesoscale synoptic conditions, J. Geophys. Res.-Atmos., 15, D17302, https://doi.org/10.1029/2010JD013940, 2010.

Jaeglé, L., Quinn, P. K., Bates, T. S., Alexander, B., and Lin, J.-T.: Global distribution of sea salt aerosols: new constraints from in situ and remote sensing observations, Atmos. Chem. Phys., 11, 3137–3157, https://doi.org/10.5194/acp-11-3137-2011, 2011.

Jones, A. E., Anderson, P. S., Begoin, M., Brough, N., Hutterli, M. A., Marshall, G. J., Richter, A., Roscoe, H. K., and Wolff, E. W.: BrO, blizzards, and drivers of polar tropospheric ozone depletion events, Atmos. Chem. Phys., 9, 4639–4652, https://doi.org/10.5194/acp-9-4639-2009, 2009.

Kaleschke, L., Richter, A., Burrows, J., Afe, O., Heygster, G., Notholt, J., Rankin, A. M., Roscoe, H. K., Hollwedel, J., Wagner, T., and Jacobi, H. W.: Frost flowers on sea ice as a source of sea salt and their influence on tropospheric halogen chemistry, Geophys. Res. Lett., 31, L16114, https://doi.org/10.1029/2004GL020655, 2004.

Keene, W. C., Stutz, J., Pszenny, A. A. P., Maben, J. R., Fischer, E. V., Smith, A. M., von Glasow, R., Pechtl, S., Sive, B. C., and Varner, R. K.: Inorganic chlorine and bromine in coastal New England air during summer, J. Geophys. Res.-Atmos., 112, DS10S12, https://doi.org/10.1029/2006JD007689, 2007.

Koo, J.-H., Wang, Y., Kurosu, T. P., Chance, K., Rozanov, A., Richter, A., Oltmans, S. J., Thompson, A. M., Hair, J. W., Fenn, M. A., Weinheimer, A. J., Ryerson, T. B., Solberg, S., Huey, L. G., Liao, J., Dibb, J. E., Neuman, J. A., Nowak, J. B., Pierce, R. B., Natarajan, M., and Al-Saadi, J.: Characteristics of tropospheric ozone depletion events in the Arctic spring: analysis of the ARCTAS, ARCPAC, and ARCIONS measurements and satellite BrO observations, Atmos. Chem. Phys., 12, 9909–9922, https://doi.org/10.5194/acp-12-9909-2012, 2012.

Koop, T., Kapilashrami, A., Molina, L. T., and Molina, M. J.: Phase transitions of sea-salt/water mixtures at low temperatures: Implications for ozone chemistry in the polar marine boundary layer, J. Geophys. Res.-Atmos., 105, 26393–26402, https://doi.org/10.1029/2000JD900413, 2000.

Krnavek, L., Simpson, W. R., Carlson, D., Domine, F., Douglas, T. A., and Sturm, M.: The chemical composition of surface snow in the Arctic: Examining marine, terrestrial, and atmospheric influences, Atmos. Environ., 50, 349–359, https://doi.org/10.1016/j.atmosenv.2011.11.033, 2012.

Kwok, R. and Cunningham, G. F.: ICESat over Arctic sea ice: Estimation of snow depth and ice thickness, J. Geophys. Res.-Oceans, 113, C08010, https://doi.org/10.1029/2008JC004753, 2008.

Lehrer, E., Hönninger, G., and Platt, U.: A one dimensional model study of the mechanism of halogen liberation and vertical transport in the polar troposphere, Atmos. Chem. Phys., 4, 2427–2440, https://doi.org/10.5194/acp-4-2427-2004, 2004.

Levelt, P. F., Oord, G. H. J. van den, Dobber, M. R., Malkki, A., Visser, H., Vries, J. de, Stammes, P., Lundell, J. O. V., and Saari, H.: The ozone monitoring instrument, IEEE T. Geosci. Remote, 44, 1093–1101, https://doi.org/10.1109/TGRS.2006.872333, 2006.

Lewis, E. R. and Schwartz, S. E.: Fundamentals, in Sea Salt Aerosol Production: Mechanisms, Methods, Measurements and Models, American Geophysical Union (AGU), Washington, D.C., USA, 9–99, 2004.

Liao, J., Huey, L. G., Scheuer, E., Dibb, J. E., Stickel, R. E., Tanner, D. J., Neuman, J. A., Nowak, J. B., Choi, S., Wang, Y., Salawitch, R. J., Canty, T., Chance, K., Kurosu, T., Suleiman, R., Weinheimer, A. J., Shetter, R. E., Fried, A., Brune, W., Anderson, B., Zhang, X., Chen, G., Crawford, J., Hecobian, A., and Ingall, E. D.: Characterization of soluble bromide measurements and a case study of BrO observations during ARCTAS, Atmos. Chem. Phys., 12, 1327–1338, https://doi.org/10.5194/acp-12-1327-2012, 2012.

Lindsay, R., Wensnahan, M., Schweiger, A., and Zhang, J.: Evaluation of Seven Different Atmospheric Reanalysis Products in the Arctic, J. Climate, 27, 2588–2606, https://doi.org/10.1175/JCLI-D-13-00014.1, 2014.

Macdonald, K. M., Sharma, S., Toom, D., Chivulescu, A., Hanna, S., Bertram, A. K., Platt, A., Elsasser, M., Huang, L., Tarasick, D., Chellman, N., McConnell, J. R., Bozem, H., Kunkel, D., Lei, Y. D., Evans, G. J., and Abbatt, J. P. D.: Observations of atmospheric chemical deposition to high Arctic snow, Atmos. Chem. Phys., 17, 5775–5788, https://doi.org/10.5194/acp-17-5775-2017, 2017.

Mao, J., Paulot, F., Jacob, D. J., Cohen, R. C., Crounse, J. D., Wennberg, P. O., Keller, C. A., Hudman, R. C., Barkley, M. P., and Horowitz, L. W.: Ozone and organic nitrates over the eastern United States: Sensitivity to isoprene chemistry, J. Geophys. Res.-Atmos., 118, 11256–11268, https://doi.org/10.1002/jgrd.50817, 2013.

McConnell, J. C., Henderson, G. S., Barrie, L., Bottenheim, J., Niki, H., Langford, C. H., and Templeton, E. M. J.: Photochemical bromine production implicated in Arctic boundary-layer ozone depletion, Nature, 355, 150–152, https://doi.org/10.1038/355150a0, 1992.

Moore, C. W., Obrist, D., Steffen, A., Staebler, R. M., Douglas, T. A., Richter, A., and Nghiem, S. V.: Convective forcing of mercury and ozone in the Arctic boundary layer induced by leads in sea ice, Nature, 506, 81–83, https://doi.org/10.1038/nature12924, 2014.

Morin, S., Honninger, G. H., Staebler, R. M., and Bottenheim, J. W.: A high time resolution study of boundary layer ozone chemistry and dynamics over the Arctic Ocean near Alert, Nunavut, Geophys. Res. Lett., 32, L08809, https://doi.org/10.1029/2004GL022098, 2005.

Morin, S., Marion, G. M., von Glasow, R., Voisin, D., Bouchez, J., and Savarino, J.: Precipitation of salts in freezing seawater and ozone depletion events: a status report, Atmos. Chem. Phys., 8, 7317–7324, https://doi.org/10.5194/acp-8-7317-2008, 2008.

Munro, M., Eisinger, M., Anderson, C., Callies, J., Corpaccioli, E., Lang, R., Lefebvre, A., Livschitz, Y., and Albinana, A. P.: GOME-2 on MetOp, Proc. of The 2006 EUMETSAT Meteorological Satellite Conference, 12–16 June 2006, Helsinki, Finland, vol. 1216, p. 48, 2006.

Nandan, V., Geldsetzer, T., Yackel, J., Mahmud, M., Scharien, R., Howell, S., King, J., Ricker, R., and Else, B.: Effect of Snow Salinity on CryoSat-2 Arctic First-Year Sea Ice Freeboard Measurements, Geophys. Res. Lett., 44, 10419–10426, https://doi.org/10.1002/2017GL074506, 2017.

Neuman, J. A., Nowak, J. B., Huey, L. G., Burkholder, J. B., Dibb, J. E., Holloway, J. S., Liao, J., Peischl, J., Roberts, J. M., Ryerson, T. B., Scheuer, E., Stark, H., Stickel, R. E., Tanner, D. J., and Weinheimer, A.: Bromine measurements in ozone depleted air over the Arctic Ocean, Atmos. Chem. Phys., 10, 6503–6514, https://doi.org/10.5194/acp-10-6503-2010, 2010.

Nghiem, S. V., Rigor, I. G., Richter, A., Burrows, J. P., Shepson, P. B., Bottenheim, J., Barber, D. G., Steffen, A., Latonas, J., Wang, F., Stern, G., Clemente-Colon, P., Martin, S., Hall, D. K., Kaleschke, L., Tackett, P., Neumann, G., and Asplin, M. G.: Field and satellite observations of the formation and distribution of Arctic atmospheric bromine above a rejuvenated sea ice cover, J. Geophys. Res.-Atmos., 117, D00S05, https://doi.org/10.1029/2011JD016268, 2012.

NOAA/USDA: The Easter Freeze of April 2007, available at: https://www1.ncdc.noaa.gov/pub/data/techrpts/tr200801/tech-report-200801.pdf (last access: 31 August 2019), 2008.

Olivier, J. G. J. and Berdowski, J. J. M.: Global emissions sources and sinks, in: The Climate System, edited by: Berdowski, J., Guicherit, R., and Heij, B. J., A.A. Balkema Publishers/Swets & Zeitlinger Publishers, Lisse, the Netherlands, 33–78, 2001.

Oltmans, S. J. and Komhyr, W. D.: Surface ozone distributions and variations from 1973–1984: Measurements at the NOAA Geophysical Monitoring for Climatic Change Baseline Observatories, J. Geophys. Res.-Atmos., 91, 5229–5236, https://doi.org/10.1029/JD091iD04p05229, 1986.

Oltmans, S. J., Johnson, B. J., and Harris, J. M.: Springtime boundary layer ozone depletion at Barrow, Alaska: Meteorological influence, year-to-year variation, and long-term change, J. Geophys. Res.-Atmos., 117, D00R18, https://doi.org/10.1029/2011JD016889, 2012.

Parrella, J. P., Jacob, D. J., Liang, Q., Zhang, Y., Mickley, L. J., Miller, B., Evans, M. J., Yang, X., Pyle, J. A., Theys, N., and Van Roozendael, M.: Tropospheric bromine chemistry: implications for present and pre-industrial ozone and mercury, Atmos. Chem. Phys., 12, 6723–6740, https://doi.org/10.5194/acp-12-6723-2012, 2012.

Peterson, P. K., Simpson, W. R., Pratt, K. A., Shepson, P. B., Frieß, U., Zielcke, J., Platt, U., Walsh, S. J., and Nghiem, S. V.: Dependence of the vertical distribution of bromine monoxide in the lower troposphere on meteorological factors such as wind speed and stability, Atmos. Chem. Phys., 15, 2119–2137, https://doi.org/10.5194/acp-15-2119-2015, 2015.

Peterson, P. K., Pöhler, D., Sihler, H., Zielcke, J., General, S., Frieß, U., Platt, U., Simpson, W. R., Nghiem, S. V., Shepson, P. B., Stirm, B. H., Dhaniyala, S., Wagner, T., Caulton, D. R., Fuentes, J. D., and Pratt, K. A.: Observations of bromine monoxide transport in the Arctic sustained on aerosol particles, Atmos. Chem. Phys., 17, 7567–7579, https://doi.org/10.5194/acp-17-7567-2017, 2017.

Peterson, P. K., Pöhler, D., Zielcke, J., General, S., Frieß, U., Platt, U., Simpson, W. R., Nghiem, S. V., Shepson, P. B., Stirm, B. H., and Pratt, K. A.: Springtime Bromine Activation over Coastal and Inland Arctic Snowpacks, ACS Earth Space Chem., 2, 1075–1086, https://doi.org/10.1021/acsearthspacechem.8b00083, 2018.

Peterson, P. K., Hartwig, M., May, N. W., Schwartz, E., Rigor, I., Ermold, W., Steele, M., Morison, J. H., Nghiem, S. V., and Pratt, K. A.: Snowpack measurements suggest role for multi-year sea ice regions in Arctic atmospheric bromine and chlorine chemistry, Elem. Sci. Anth., 7, 14, https://doi.org/10.1525/elementa.352, 2019.

Petty, A. A., Webster, M., Boisvert, L., and Markus, T.: The NASA Eulerian Snow on Sea Ice Model (NESOSIM) v1.0: initial model development and analysis, Geosci. Model Dev., 11, 4577–4602, https://doi.org/10.5194/gmd-11-4577-2018, 2018.

Piot, M. and von Glasow, R.: The potential importance of frost flowers, recycling on snow, and open leads for ozone depletion events, Atmos. Chem. Phys., 8, 2437–2467, https://doi.org/10.5194/acp-8-2437-2008, 2008.

Pratt, K. A., Custard, K. D., Shepson, P. B., Douglas, T. A., Poehler, D., General, S., Zielcke, J., Simpson, W. R., Platt, U., Tanner, D. J., Huey, L. G., Carlsen, M., and Stirm, B. H.: Photochemical production of molecular bromine in Arctic surface snowpacks, Nat. Geosci., 6, 351–356, https://doi.org/10.1038/NGEO1779, 2013.

Rankin, A. M., Wolff, E. W., and Martin, S.: Frost flowers: Implications for tropospheric chemistry and ice core interpretation, J. Geophys. Res.-Atmos., 107, AAC 4-1–AAC 4-15, https://doi.org/10.1029/2002JD002492, 2002.

Rhodes, R. H., Yang, X., Wolff, E. W., McConnell, J. R., and Frey, M. M.: Sea ice as a source of sea salt aerosol to Greenland ice cores: a model-based study, Atmos. Chem. Phys., 17, 9417–9433, https://doi.org/10.5194/acp-17-9417-2017, 2017.

Richter, A., Wittrock, F., Eisinger, M., and Burrows, J. P.: GOME observations of tropospheric BrO in northern hemispheric spring and summer 1997, Geophys. Res. Lett., 25, 2683–2686, https://doi.org/10.1029/98GL52016, 1998.

Ridley, B. A., Zeng, T., Wang, Y., Atlas, E. L., Browell, E. V., Hess, P. G., Orlando, J. J., Chance, K., and Richter, A.: An ozone depletion event in the sub-arctic surface layer over Hudson Bay, Canada, J. Atmos. Chem., 57, 255–280, https://doi.org/10.1007/s10874-007-9072-z, 2007.

Roscoe, H. K., Brooks, B., Jackson, A. V., Smith, M. H., Walker, S. J., Obbard, R. W., and Wolff, E. W.: Frost flowers in the laboratory: Growth, characteristics, aerosol, and the underlying sea ice, J. Geophys. Res.-Atmos., 116, DS12301, https://doi.org/10.1029/2010JD015144, 2011.

Salawitch, R. J., Canty, T., Kurosu, T., Chance, K., Liang, Q., da Silva, A., Pawson, S., Nielsen, J. E., Rodriguez, J. M., Bhartia, P. K., Liu, X., Huey, L. G., Liao, J., Stickel, R. E., Tanner, D. J., Dibb, J. E., Simpson, W. R., Donohoue, D., Weinheimer, A., Flocke, F., Knapp, D., Montzka, D., Neuman, J. A., Nowak, J. B., Ryerson, T. B., Oltmans, S., Blake, D. R., Atlas, E. L., Kinnison, D. E., Tilmes, S., Pan, L. L., Hendrick, F., Van Roozendael, M., Kreher, K., Johnston, P. V., Gao, R. S., Johnson, B., Bui, T. P., Chen, G., Pierce, R. B., Crawford, J. H., and Jacob, D. J.: A new interpretation of total column BrO during Arctic spring, Geophys. Res. Lett., 37, L21805, https://doi.org/10.1029/2010GL043798, 2010.

Sander, R., Keene, W. C., Pszenny, A. A. P., Arimoto, R., Ayers, G. P., Baboukas, E., Cainey, J. M., Crutzen, P. J., Duce, R. A., Hönninger, G., Huebert, B. J., Maenhaut, W., Mihalopoulos, N., Turekian, V. C., and Van Dingenen, R.: Inorganic bromine in the marine boundary layer: a critical review, Atmos. Chem. Phys., 3, 1301–1336, https://doi.org/10.5194/acp-3-1301-2003, 2003.

Schmidt, J. A., Jacob D. J., Horowitz H. M., Hu L., Sherwen T., Evans M. J., Liang Q., Suleiman R. M., Oram D. E., Le Breton M., Percival C. J., Wang S., Dix B., and Volkamer R.: Modeling the observed tropospheric BrO background: Importance of multiphase chemistry and implications for ozone, OH, and mercury, J. Geophys. Res.-Atmos., 121, 11819–11835, https://doi.org/10.1002/2015JD024229, 2016.

Schroeder, W. H., Anlauf, K. G., Barrie, L. A., Lu, J. Y., Steffen, A., Schneeberger, D. R., and Berg, T.: Arctic springtime depletion of mercury, Nature, 394, 331–332, https://doi.org/10.1038/28530, 1998.

Seabrook, J. A., Whiteway, J., Staebler, R. M., Bottenheim, J. W., Komguem, L., Gray, L. H., Barber, D., and Asplin, M.: LIDAR measurements of Arctic boundary layer ozone depletion events over the frozen Arctic Ocean, J. Geophys. Res.-Atmos., 116, DS00S02, https://doi.org/10.1029/2011JD016335, 2011.

Sherwen, T., Schmidt, J. A., Evans, M. J., Carpenter, L. J., Großmann, K., Eastham, S. D., Jacob, D. J., Dix, B., Koenig, T. K., Sinreich, R., Ortega, I., Volkamer, R., Saiz-Lopez, A., Prados-Roman, C., Mahajan, A. S., and Ordóñez, C.: Global impacts of tropospheric halogens (Cl, Br, I) on oxidants and composition in GEOS-Chem, Atmos. Chem. Phys., 16, 12239–12271, https://doi.org/10.5194/acp-16-12239-2016, 2016a.

Sherwen, T., Evans, M. J., Carpenter, L. J., Andrews, S. J., Lidster, R. T., Dix, B., Koenig, T. K., Sinreich, R., Ortega, I., Volkamer, R., Saiz-Lopez, A., Prados-Roman, C., Mahajan, A. S., and Ordóñez, C.: Iodine's impact on tropospheric oxidants: a global model study in GEOS-Chem, Atmos. Chem. Phys., 16, 1161–1186, https://doi.org/10.5194/acp-16-1161-2016, 2016b.

Simpson, W. R., Alvarez-Aviles, L., Douglas, T. A., Sturm, M., and Domine, F.: Halogens in the coastal snow pack near Barrow, Alaska: Evidence for active bromine air-snow chemistry during springtime, Geophys. Res. Lett., 32, L04811, https://doi.org/10.1029/2004GL021748, 2005.

Simpson, W. R., Carlson, D., Hönninger, G., Douglas, T. A., Sturm, M., Perovich, D., and Platt, U.: First-year sea-ice contact predicts bromine monoxide (BrO) levels at Barrow, Alaska better than potential frost flower contact, Atmos. Chem. Phys., 7, 621–627, https://doi.org/10.5194/acp-7-621-2007, 2007a.

Simpson, W. R., von Glasow, R., Riedel, K., Anderson, P., Ariya, P., Bottenheim, J., Burrows, J., Carpenter, L. J., Frieß, U., Goodsite, M. E., Heard, D., Hutterli, M., Jacobi, H.-W., Kaleschke, L., Neff, B., Plane, J., Platt, U., Richter, A., Roscoe, H., Sander, R., Shepson, P., Sodeau, J., Steffen, A., Wagner, T., and Wolff, E.: Halogens and their role in polar boundary-layer ozone depletion, Atmos. Chem. Phys., 7, 4375–4418, https://doi.org/10.5194/acp-7-4375-2007, 2007b.

Simpson, W. R., Peterson, P. K., Frieß, U., Sihler, H., Lampel, J., Platt, U., Moore, C., Pratt, K., Shepson, P., Halfacre, J., and Nghiem, S. V.: Horizontal and vertical structure of reactive bromine events probed by bromine monoxide MAX-DOAS, Atmos. Chem. Phys., 17, 9291–9309, https://doi.org/10.5194/acp-17-9291-2017, 2017.

Spolaor, A., Gabrieli, J., Martma, T., Kohler, J., Björkman, M. B., Isaksson, E., Varin, C., Vallelonga, P., Plane, J. M. C., and Barbante, C.: Sea ice dynamics influence halogen deposition to Svalbard, The Cryosphere, 7, 1645–1658, https://doi.org/10.5194/tc-7-1645-2013, 2013.

Spolaor, A., Vallelonga, P., Gabrieli, J., Martma, T., Björkman, M. P., Isaksson, E., Cozzi, G., Turetta, C., Kjær, H. A., Curran, M. A. J., Moy, A. D., Schönhardt, A., Blechschmidt, A.-M., Burrows, J. P., Plane, J. M. C., and Barbante, C.: Seasonality of halogen deposition in polar snow and ice, Atmos. Chem. Phys., 14, 9613–9622, https://doi.org/10.5194/acp-14-9613-2014, 2014.

Steffen, A., Douglas, T., Amyot, M., Ariya, P., Aspmo, K., Berg, T., Bottenheim, J., Brooks, S., Cobbett, F., Dastoor, A., Dommergue, A., Ebinghaus, R., Ferrari, C., Gardfeldt, K., Goodsite, M. E., Lean, D., Poulain, A. J., Scherz, C., Skov, H., Sommar, J., and Temme, C.: A synthesis of atmospheric mercury depletion event chemistry in the atmosphere and snow, Atmos. Chem. Phys., 8, 1445–1482, https://doi.org/10.5194/acp-8-1445-2008, 2008.

Tarasick, D. W. and Bottenheim, J. W.: Surface ozone depletion episodes in the Arctic and Antarctic from historical ozonesonde records, Atmos. Chem. Phys., 2, 197–205, https://doi.org/10.5194/acp-2-197-2002, 2002.

Theys, N., Van Roozendael, M., Errera, Q., Hendrick, F., Daerden, F., Chabrillat, S., Dorf, M., Pfeilsticker, K., Rozanov, A., Lotz, W., Burrows, J. P., Lambert, J.-C., Goutail, F., Roscoe, H. K., and De Mazière, M.: A global stratospheric bromine monoxide climatology based on the BASCOE chemical transport model, Atmos. Chem. Phys., 9, 831–848, https://doi.org/10.5194/acp-9-831-2009, 2009.

Theys, N., Van Roozendael, M., Hendrick, F., Yang, X., De Smedt, I., Richter, A., Begoin, M., Errera, Q., Johnston, P. V., Kreher, K., and De Mazière, M.: Global observations of tropospheric BrO columns using GOME-2 satellite data, Atmos. Chem. Phys., 11, 1791–1811, https://doi.org/10.5194/acp-11-1791-2011, 2011.

Toom-Sauntry, D. and Barrie, L. A.: Chemical composition of snowfall in the high Arctic: 1990–1994, Atmos. Environ., 36, 2683–2693, https://doi.org/10.1016/S1352-2310(02)00115-2, 2002.

Toyota, K., McConnell, J. C., Lupu, A., Neary, L., McLinden, C. A., Richter, A., Kwok, R., Semeniuk, K., Kaminski, J. W., Gong, S.-L., Jarosz, J., Chipperfield, M. P., and Sioris, C. E.: Analysis of reactive bromine production and ozone depletion in the Arctic boundary layer using 3-D simulations with GEM-AQ: inference from synoptic-scale patterns, Atmos. Chem. Phys., 11, 3949–3979, https://doi.org/10.5194/acp-11-3949-2011, 2011.

Travis, K. R., Jacob, D. J., Fisher, J. A., Kim, P. S., Marais, E. A., Zhu, L., Yu, K., Miller, C. C., Yantosca, R. M., Sulprizio, M. P., Thompson, A. M., Wennberg, P. O., Crounse, J. D., St. Clair, J. M., Cohen, R. C., Laughner, J. L., Dibb, J. E., Hall, S. R., Ullmann, K., Wolfe, G. M., Pollack, I. B., Peischl, J., Neuman, J. A., and Zhou, X.: Why do models overestimate surface ozone in the Southeast United States?, Atmos. Chem. Phys., 16, 13561–13577, https://doi.org/10.5194/acp-16-13561-2016, 2016.

Uotila, P., Goosse, H., Haines, K., Chevallier, M., Barthélemy, A., Bricaud, C., Carton, J., Fučkar, N., Garric, G., Iovino, D., Kauker, F., Korhonen, M., Lien, V. S., Marnela, M., Massonnet, F., Mignac, D., Peterson, K. A., Sadikni, R., Shi, L., Tietsche, S., Toyoda, T., Xie, J., and Zhang, Z.: An assessment of ten ocean reanalyses in the polar regions, Clim. Dynam., 52, 1613–1650, https://doi.org/10.1007/s00382-018-4242-z, 2019.

van der Werf, G. R., Randerson, J. T., Giglio, L., van Leeuwen, T. T., Chen, Y., Rogers, B. M., Mu, M., van Marle, M. J. E., Morton, D. C., Collatz, G. J., Yokelson, R. J., and Kasibhatla, P. S.: Global fire emissions estimates during 1997–2016, Earth Syst. Sci. Data, 9, 697–720, https://doi.org/10.5194/essd-9-697-2017, 2017.

Wagner, T., Leue, C., Wenig, M., Pfeilsticker, K., and Platt, U.: Spatial and temporal distribution of enhanced boundary layer BrO concentrations measured by the GOME instrument aboard ERS-2, J. Geophys. Res.-Atmos., 106, 24225–24235, https://doi.org/10.1029/2000JD000201, 2001.

Wagner, T., Ibrahim, O., Sinreich, R., Frieß, U., von Glasow, R., and Platt, U.: Enhanced tropospheric BrO over Antarctic sea ice in mid winter observed by MAX-DOAS on board the research vessel Polarstern, Atmos. Chem. Phys., 7, 3129–3142, https://doi.org/10.5194/acp-7-3129-2007, 2007.

Wang, S., McNamara, S. M., Moore, C. W., Obrist, D., Steffen, A., Shepson, P. B., Staebler, R. M., Raso, A. R. W., and Pratt, K. A.: Direct detection of atmospheric atomic bromine leading to mercury and ozone depletion, P. Natl. Acad. Sci. USA, 116, 14479–14484, https://doi.org/10.1073/pnas.1900613116, 2019.

Wang, X., Jacob, D. J., Eastham, S. D., Sulprizio, M. P., Zhu, L., Chen, Q., Alexander, B., Sherwen, T., Evans, M. J., Lee, B. H., Haskins, J. D., Lopez-Hilfiker, F. D., Thornton, J. A., Huey, G. L., and Liao, H.: The role of chlorine in global tropospheric chemistry, Atmos. Chem. Phys., 19, 3981–4003, https://doi.org/10.5194/acp-19-3981-2019, 2019.

Warren, S. G., Rigor, I. G., Untersteiner, N., Radionov, V. F., Bryazgin, N. N., Aleksandrov, Y. I., and

Colony, R.: Snow Depth on Arctic Sea Ice, J. Climate, 12, 1814–1829, https://doi.org/10.1175/1520-0442(1999)012<1814:SDOASI>2.0.CO;2, 1999.

Wren, S. N., Donaldson, D. J., and Abbatt, J. P. D.: Photochemical chlorine and bromine activation from artificial saline snow, Atmos. Chem. Phys., 13, 9789–9800, https://doi.org/10.5194/acp-13-9789-2013, 2013.

Yang, X., Pyle, J. A., and Cox, R. A.: Sea salt aerosol production and bromine release: Role of snow on sea ice, Geophys. Res. Lett., 35, L16815, https://doi.org/10.1029/2008GL034536, 2008.

Yang, X., Pyle, J. A., Cox, R. A., Theys, N., and Van Roozendael, M.: Snow-sourced bromine and its implications for polar tropospheric ozone, Atmos. Chem. Phys., 10, 7763–7773, https://doi.org/10.5194/acp-10-7763-2010, 2010.

Yang, X., Neděla, V., Runštuk, J., Ondrušková, G., Krausko, J., Vetráková, Ľ., and Heger, D.: Evaporating brine from frost flowers with electron microscopy and implications for atmospheric chemistry and sea-salt aerosol formation, Atmos. Chem. Phys., 17, 6291–6303, https://doi.org/10.5194/acp-17-6291-2017, 2017.

Zhao, X., Strong, K., Adams, C., Schofield, R., Yang, X., Richter, A., Friess, U., Blechschmidt, A.-M., and Koo, J.-H.: A case study of a transported bromine explosion event in the Canadian high arctic, J. Geophys. Res.-Atmos., 121, 457–477, https://doi.org/10.1002/2015JD023711, 2016.

Zhu, L., Jacob, D. J., Eastham, S. D., Sulprizio, M. P., Wang, X., Sherwen, T., Evans, M. J., Chen, Q., Alexander, B., Koenig, T. K., Volkamer, R., Huey, L. G., Le Breton, M., Bannan, T. J., and Percival, C. J.: Effect of sea salt aerosol on tropospheric bromine chemistry, Atmos. Chem. Phys., 19, 6497–6507, https://doi.org/10.5194/acp-19-6497-2019, 2019.

Zygmuntowska, M., Rampal, P., Ivanova, N., and Smedsrud, L. H.: Uncertainties in Arctic sea ice thickness and volume: new estimates and implications for trends, The Cryosphere, 8, 705–720, https://doi.org/10.5194/tc-8-705-2014, 2014.